Supplemental Material: Chiral degeneracies and Fermi-surface Chern numbers in bcc Fe

Daniel Gosálbez-Martínez,[1,2] Ivo Souza,[1,3] and David Vanderbilt[4]

[1] *Centro de Física de Materiales, Universidad del País Vasco, 20018 San Sebastián, Spain*
[2] *Donostia International Physics Center, 20018 San Sebastián, Spain*
[3] *Ikerbasque Foundation, 48013 Bilbao, Spain*
[4] *Department of Physics and Astronomy, Rutgers University, Piscataway, New Jersey 08854-8019, USA*

Note: This PDF document contains a large number of pages and figures, and is best viewed electronically. By flipping the pages, a simple animation effect is obtained for each sequence of snapshots.

I. CHIRAL TOUCHING BETWEEN FERMI SHEETS INDUCED BY MAGNETIZATION PRECESSION

Figure S1 shows the Fermi contours of bands nine and ten of bcc Fe on the ΓNH ($k_z = 0$) plane in Fig. 3, calculated with the magnetization pointing along [001]. The blow-up on the right shows the two points of contact between sheets 9 and 10_2, located along a degeneracy loop protected by mirror symmetry (Sec. VI.B.1). Those gluing points render ill-defined the Chern numbers of the low-symmetry pockets $(10_2, 10_3, 10_4, 10_5)$, as discussed in Sec. VI.B.3.

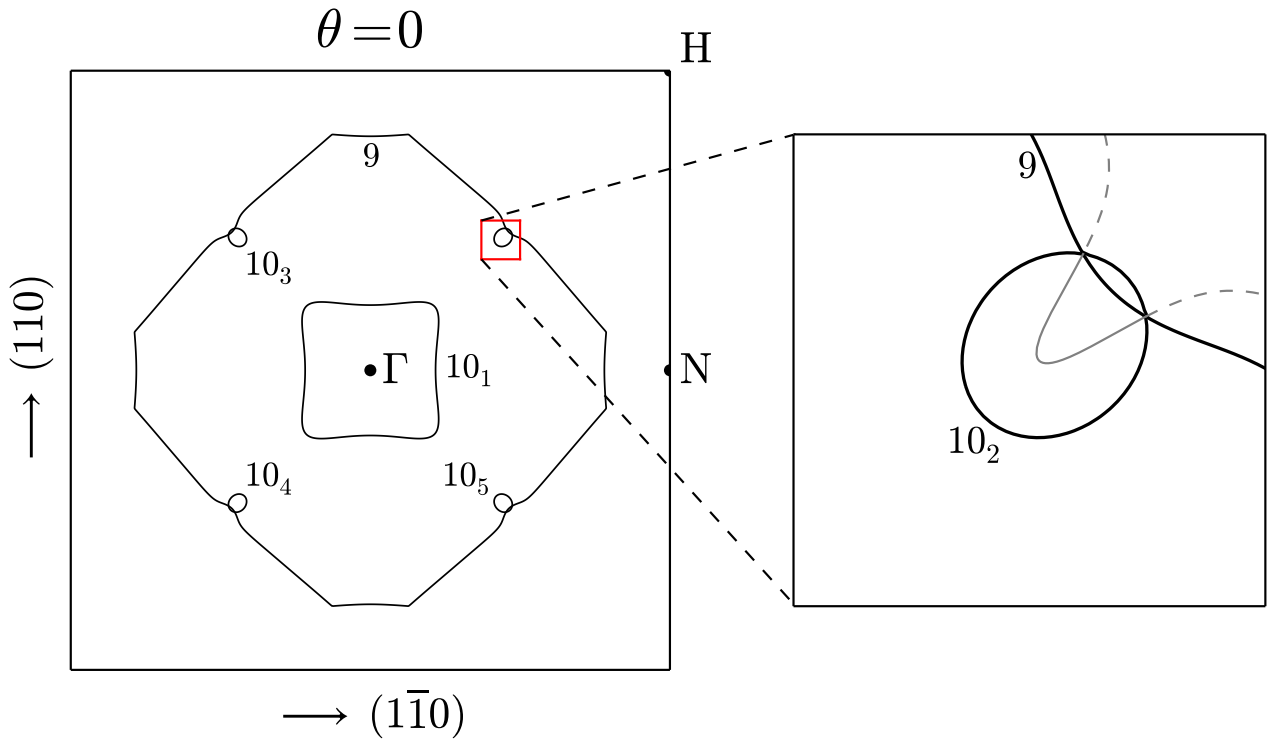

FIG. S1. Left: Fermi contours of bands nine and ten on the ΓNH Brillouin-zone slice at $k_z = 0$, with the magnetization pointing along [001] (polar angle $\theta = 0$). Right: Detail showing the gluing points between sheets 9 and 10_2 along a nodal ring. The solid-line portion of the nodal ring is below the Fermi level, and the dashed-line portions are above.

In Fig. S2 the magnetization has been tilted by 20° towards the [100] axis, breaking the mirror symmetry. As a result the nodal rings have been reduced to a few Weyl points, and the previously glued-together Fermi sheets became isolated, with well-defined Chern numbers given by the enclosed chiral charges (Sec. VI.B.3). For example, pocket 10_2 has Chern number +1, because it encloses a single touching point of negative chirality with the band below.

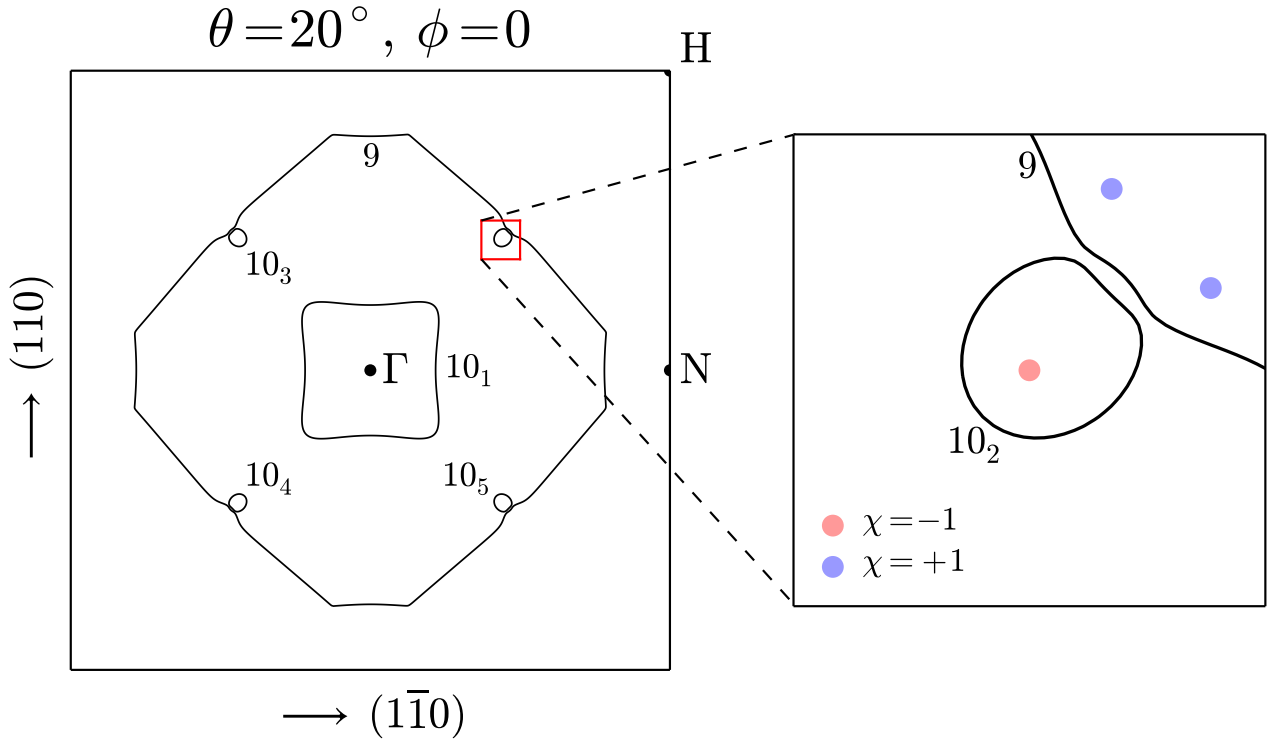

FIG. S2. Left: Fermi contours of bands nine and ten on the ΓNH Brillouin-zone slice at $k_z = 0$, with the magnetization tilted by 20° towards the [100] axis. Right: Detail showing the now-detached sheets 9 and 10_2. The nodal ring has evaporated, leaving behind a few remnant Weyl points represented by the colored disks, with chiralities χ.

The series of snapshots in Figs. S3-S19 shows the evolution of sheets 9 and 10_2, and the motion of nearby Weyl points (WPs), as the magnetization precesses around [001] (ϕ is the azimuthal precession angle). In order to see clearly the touching between the two sheets at $\phi \simeq 46°$, the Fermi contours are not drawn at exactly $k_z = 0$: in each snapshot their k_z coordinate is pinned to the WP that joins the two sheets at the critical angle (in practice k_z varies only slightly from one snapshot to the next, never deviating by more than $0.004 \times 2\pi/a$ from $k_z = 0$). The touching event leads to a transfer of Chern number between the two sheets, after which the Chern number of pocket 10_2 vanishes as it now encloses two WPs of opposite chirality. The two WPs merge together and annihilate at $\phi \simeq 50°$.

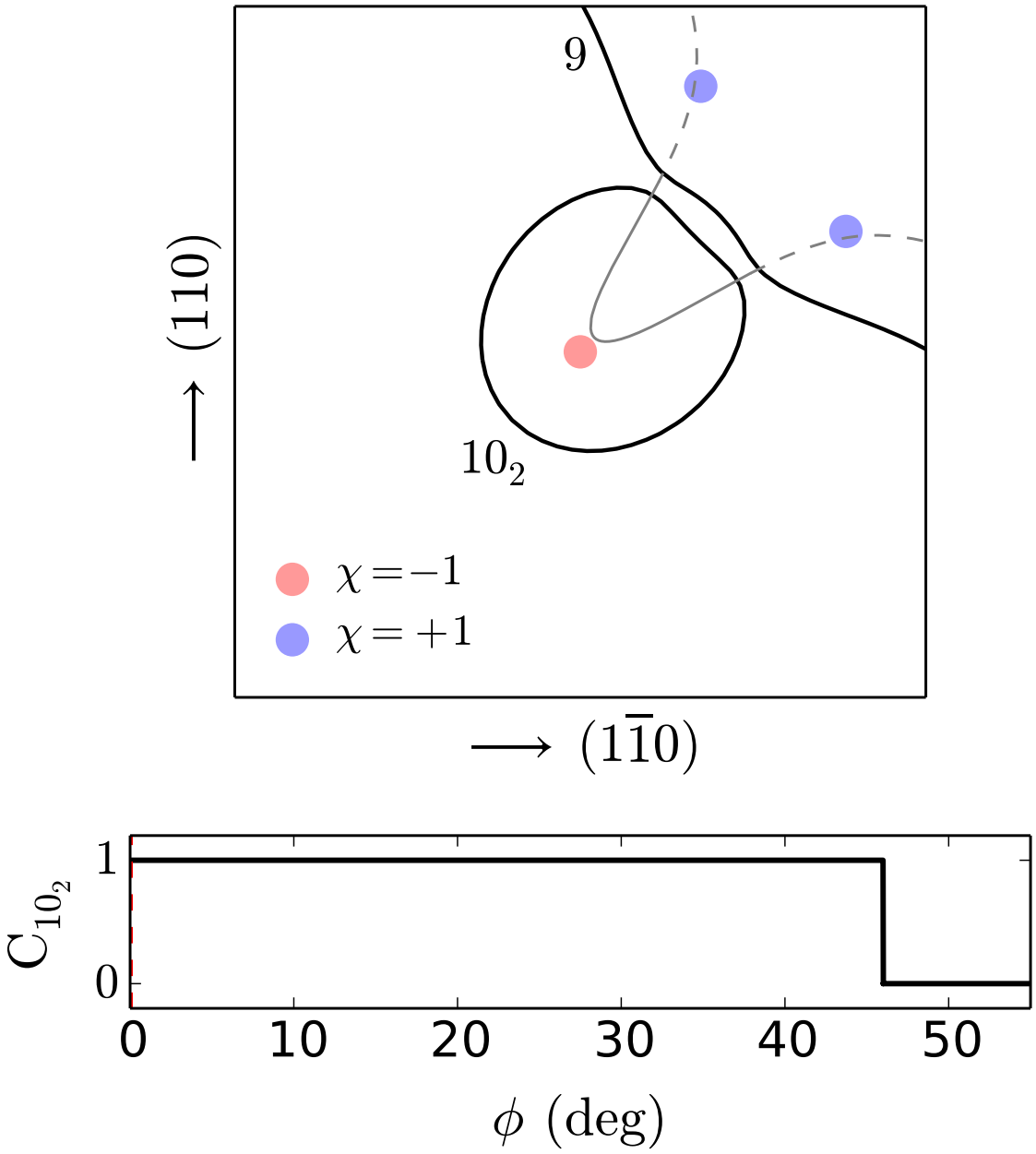

FIG. S3. Upper panel: Fermi contours of bands nine and ten, calculated with the magnetization tilted by 20° (the azimuthal angle ϕ is indicated by the dashed red line in the lower panel). The remnant Weyl points are displayed as colored disks, and the evaporated nodal ring is shown as a guide to the eye. Lower panel: Chern number of pocket 10_2 versus ϕ.

The series of snapshots in Figs. S3-S19 shows the evolution of sheets 9 and 10_2, and the motion of nearby Weyl points (WPs), as the magnetization precesses around [001] (ϕ is the azimuthal precession angle). In order to see clearly the touching between the two sheets at $\phi \simeq 46°$, the Fermi contours are not drawn at exactly $k_z = 0$: in each snapshot their k_z coordinate is pinned to the WP that joins the two sheets at the critical angle (in practice k_z varies only slightly from one snapshot to the next, never deviating by more than $0.004 \times 2\pi/a$ from $k_z = 0$). The touching event leads to a transfer of Chern number between the two sheets, after which the Chern number of pocket 10_2 vanishes as it now encloses two WPs of opposite chirality. The two WPs merge together and annihilate at $\phi \simeq 50°$.

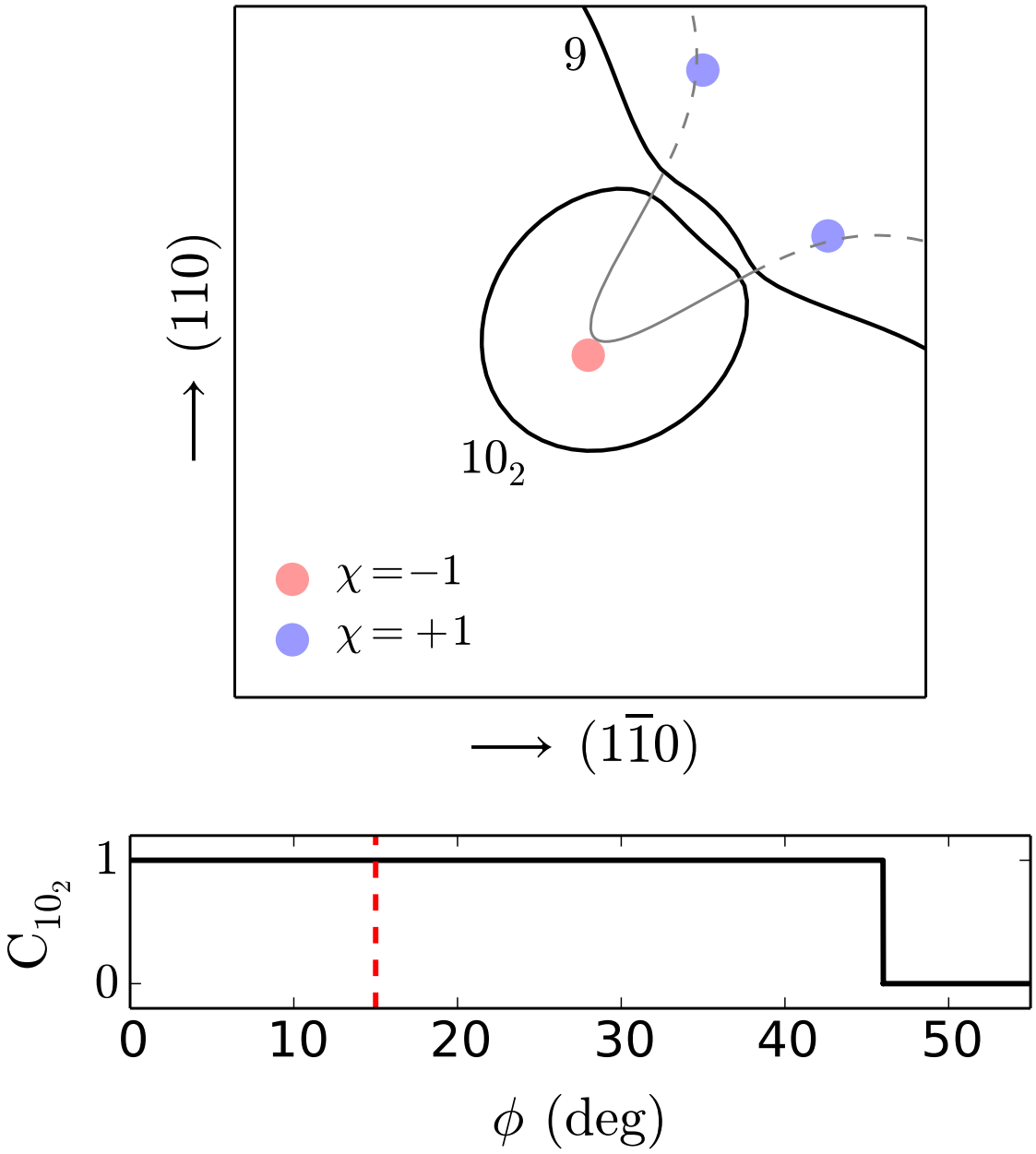

FIG. S4. Upper panel: Fermi contours of bands nine and ten, calculated with the magnetization tilted by 20° (the azimuthal angle ϕ is indicated by the dashed red line in the lower panel). The remnant Weyl points are displayed as colored disks, and the evaporated nodal ring is shown as a guide to the eye. Lower panel: Chern number of pocket 10_2 versus ϕ.

The series of snapshots in Figs. S3-S19 shows the evolution of sheets 9 and 10_2, and the motion of nearby Weyl points (WPs), as the magnetization precesses around [001] (ϕ is the azimuthal precession angle). In order to see clearly the touching between the two sheets at $\phi \simeq 46°$, the Fermi contours are not drawn at exactly $k_z = 0$: in each snapshot their k_z coordinate is pinned to the WP that joins the two sheets at the critical angle (in practice k_z varies only slightly from one snapshot to the next, never deviating by more than $0.004 \times 2\pi/a$ from $k_z = 0$). The touching event leads to a transfer of Chern number between the two sheets, after which the Chern number of pocket 10_2 vanishes as it now encloses two WPs of opposite chirality. The two WPs merge together and annihilate at $\phi \simeq 50°$.

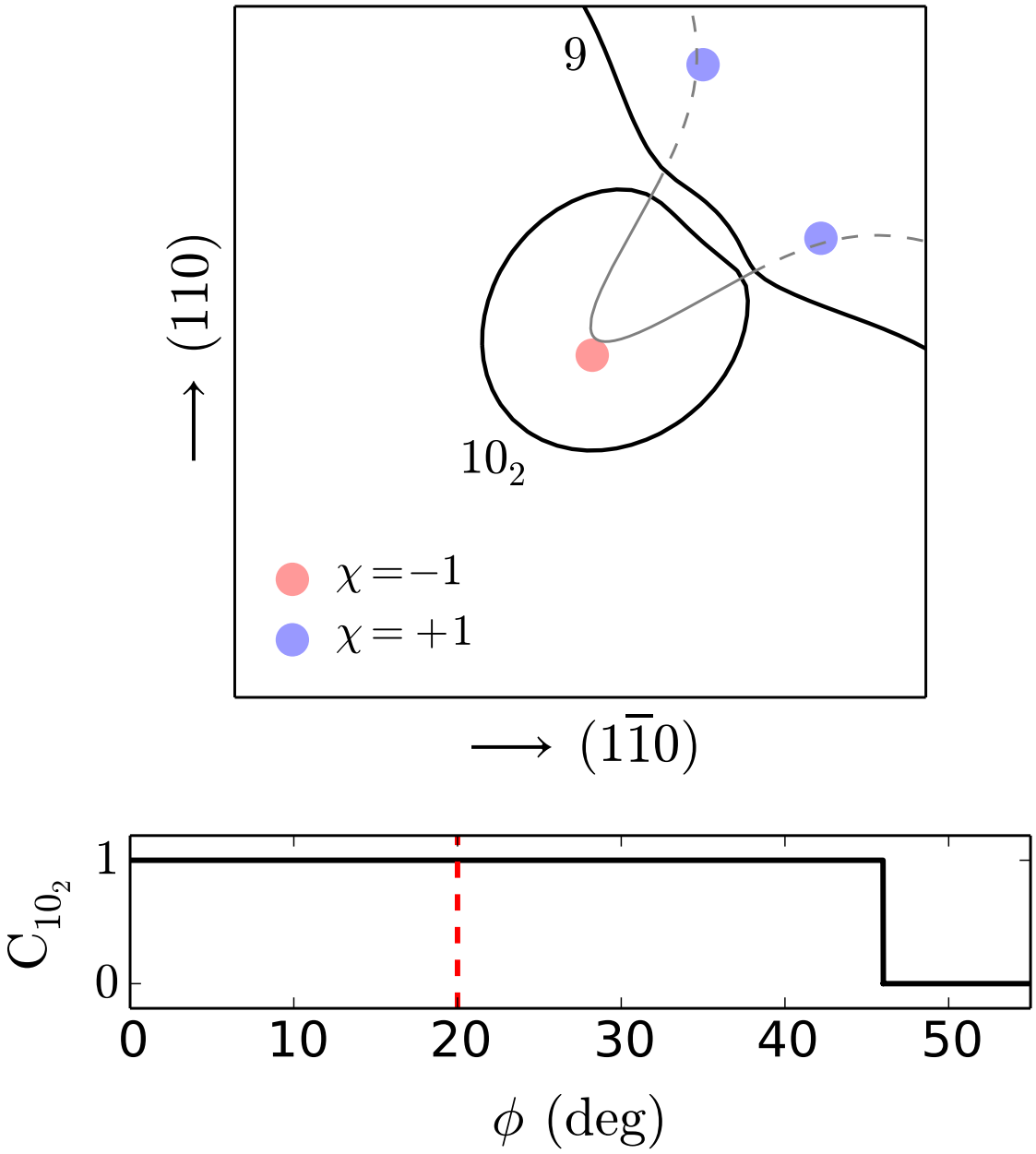

FIG. S5. Upper panel: Fermi contours of bands nine and ten, calculated with the magnetization tilted by 20° (the azimuthal angle ϕ is indicated by the dashed red line in the lower panel). The remnant Weyl points are displayed as colored disks, and the evaporated nodal ring is shown as a guide to the eye. Lower panel: Chern number of pocket 10_2 versus ϕ.

The series of snapshots in Figs. S3-S19 shows the evolution of sheets 9 and 10_2, and the motion of nearby Weyl points (WPs), as the magnetization precesses around [001] (ϕ is the azimuthal precession angle). In order to see clearly the touching between the two sheets at $\phi \simeq 46°$, the Fermi contours are not drawn at exactly $k_z = 0$: in each snapshot their k_z coordinate is pinned to the WP that joins the two sheets at the critical angle (in practice k_z varies only slightly from one snapshot to the next, never deviating by more than $0.004 \times 2\pi/a$ from $k_z = 0$). The touching event leads to a transfer of Chern number between the two sheets, after which the Chern number of pocket 10_2 vanishes as it now encloses two WPs of opposite chirality. The two WPs merge together and annihilate at $\phi \simeq 50°$.

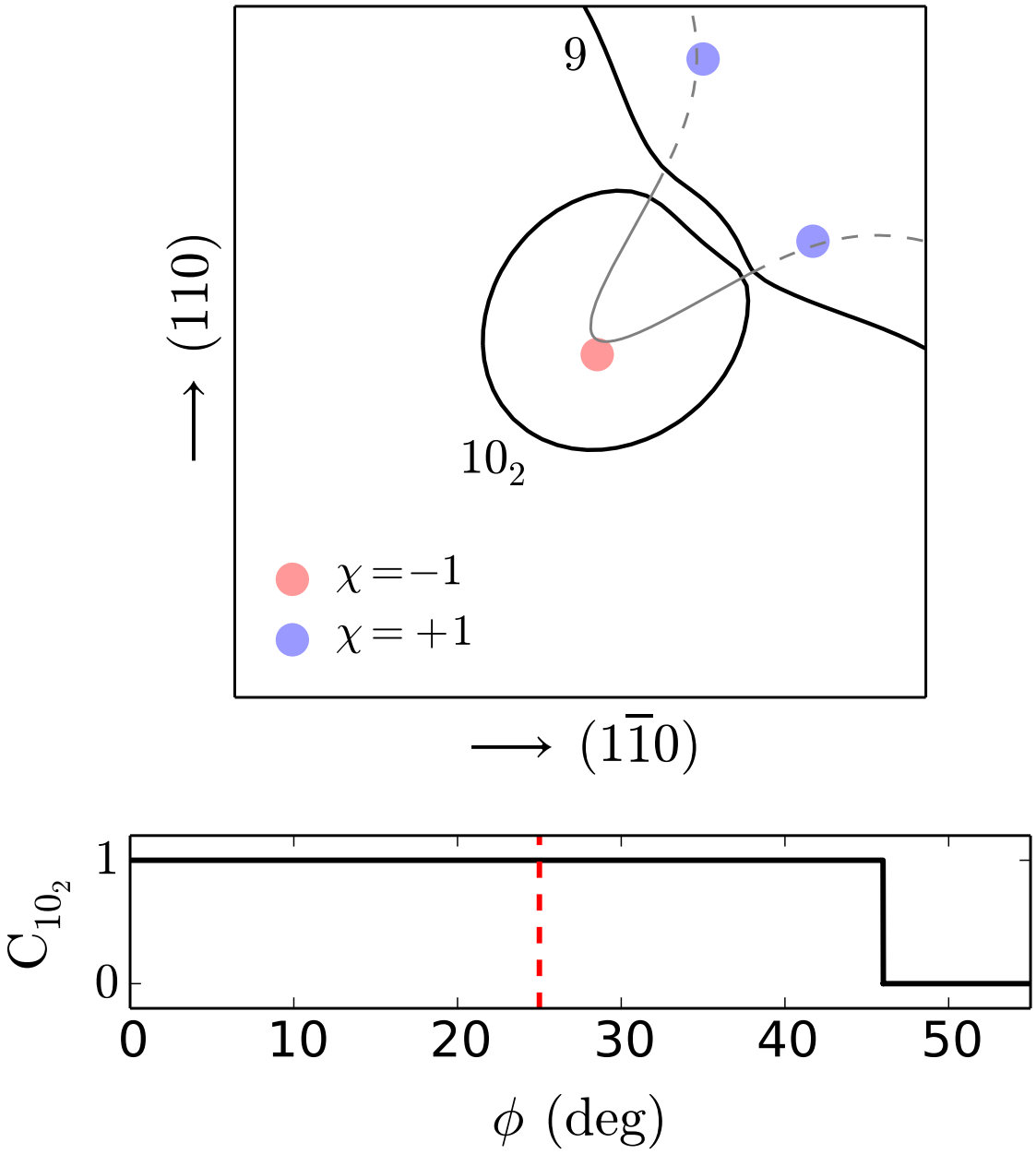

FIG. S6. Upper panel: Fermi contours of bands nine and ten, calculated with the magnetization tilted by 20° (the azimuthal angle ϕ is indicated by the dashed red line in the lower panel). The remnant Weyl points are displayed as colored disks, and the evaporated nodal ring is shown as a guide to the eye. Lower panel: Chern number of pocket 10_2 versus ϕ.

The series of snapshots in Figs. S3-S19 shows the evolution of sheets 9 and 10_2, and the motion of nearby Weyl points (WPs), as the magnetization precesses around [001] (ϕ is the azimuthal precession angle). In order to see clearly the touching between the two sheets at $\phi \simeq 46°$, the Fermi contours are not drawn at exactly $k_z = 0$: in each snapshot their k_z coordinate is pinned to the WP that joins the two sheets at the critical angle (in practice k_z varies only slightly from one snapshot to the next, never deviating by more than $0.004 \times 2\pi/a$ from $k_z = 0$). The touching event leads to a transfer of Chern number between the two sheets, after which the Chern number of pocket 10_2 vanishes as it now encloses two WPs of opposite chirality. The two WPs merge together and annihilate at $\phi \simeq 50°$.

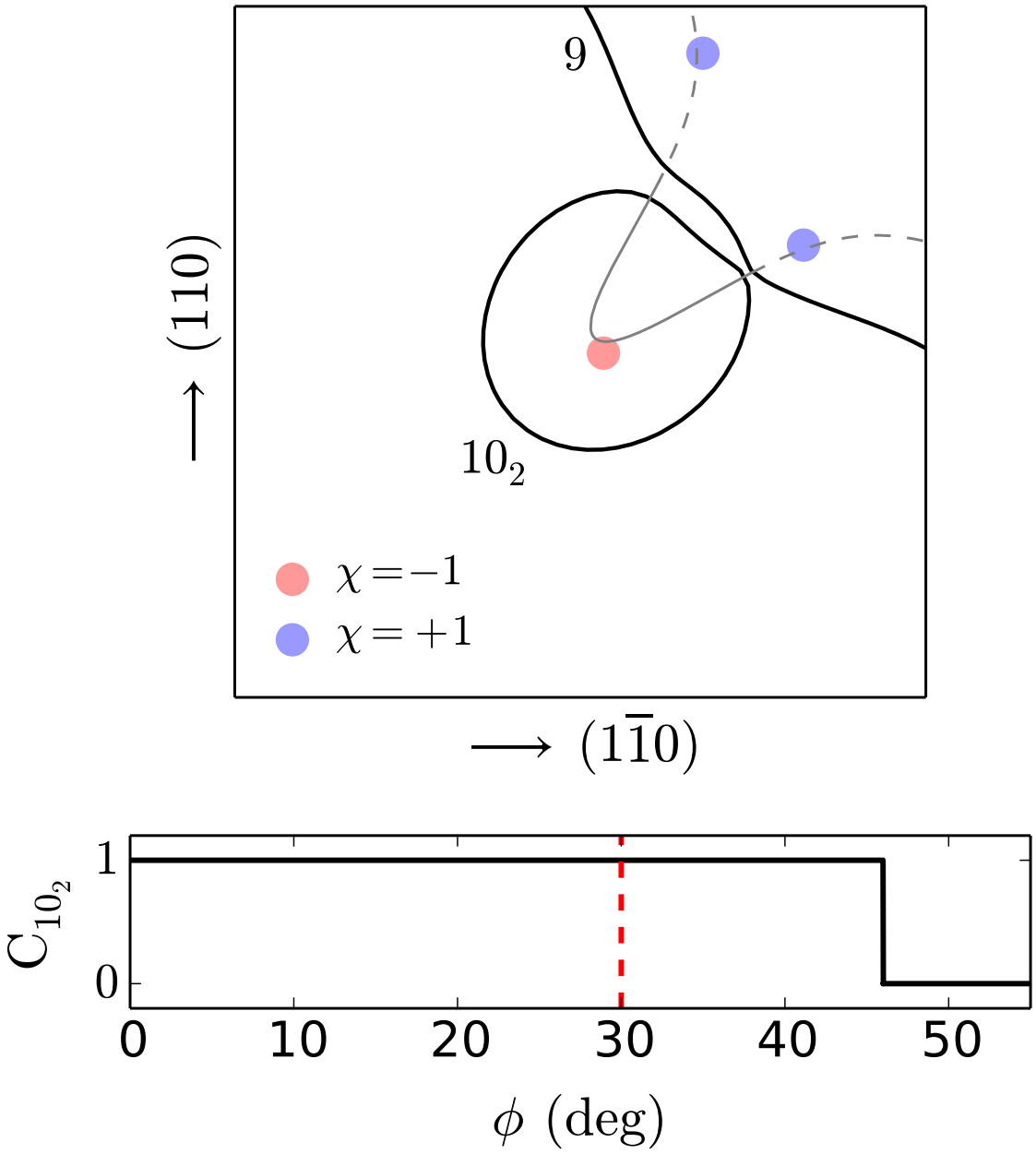

FIG. S7. Upper panel: Fermi contours of bands nine and ten, calculated with the magnetization tilted by 20° (the azimuthal angle ϕ is indicated by the dashed red line in the lower panel). The remnant Weyl points are displayed as colored disks, and the evaporated nodal ring is shown as a guide to the eye. Lower panel: Chern number of pocket 10_2 versus ϕ.

The series of snapshots in Figs. S3-S19 shows the evolution of sheets 9 and 10_2, and the motion of nearby Weyl points (WPs), as the magnetization precesses around [001] (ϕ is the azimuthal precession angle). In order to see clearly the touching between the two sheets at $\phi \simeq 46°$, the Fermi contours are not drawn at exactly $k_z = 0$: in each snapshot their k_z coordinate is pinned to the WP that joins the two sheets at the critical angle (in practice k_z varies only slightly from one snapshot to the next, never deviating by more than $0.004 \times 2\pi/a$ from $k_z = 0$). The touching event leads to a transfer of Chern number between the two sheets, after which the Chern number of pocket 10_2 vanishes as it now encloses two WPs of opposite chirality. The two WPs merge together and annihilate at $\phi \simeq 50°$.

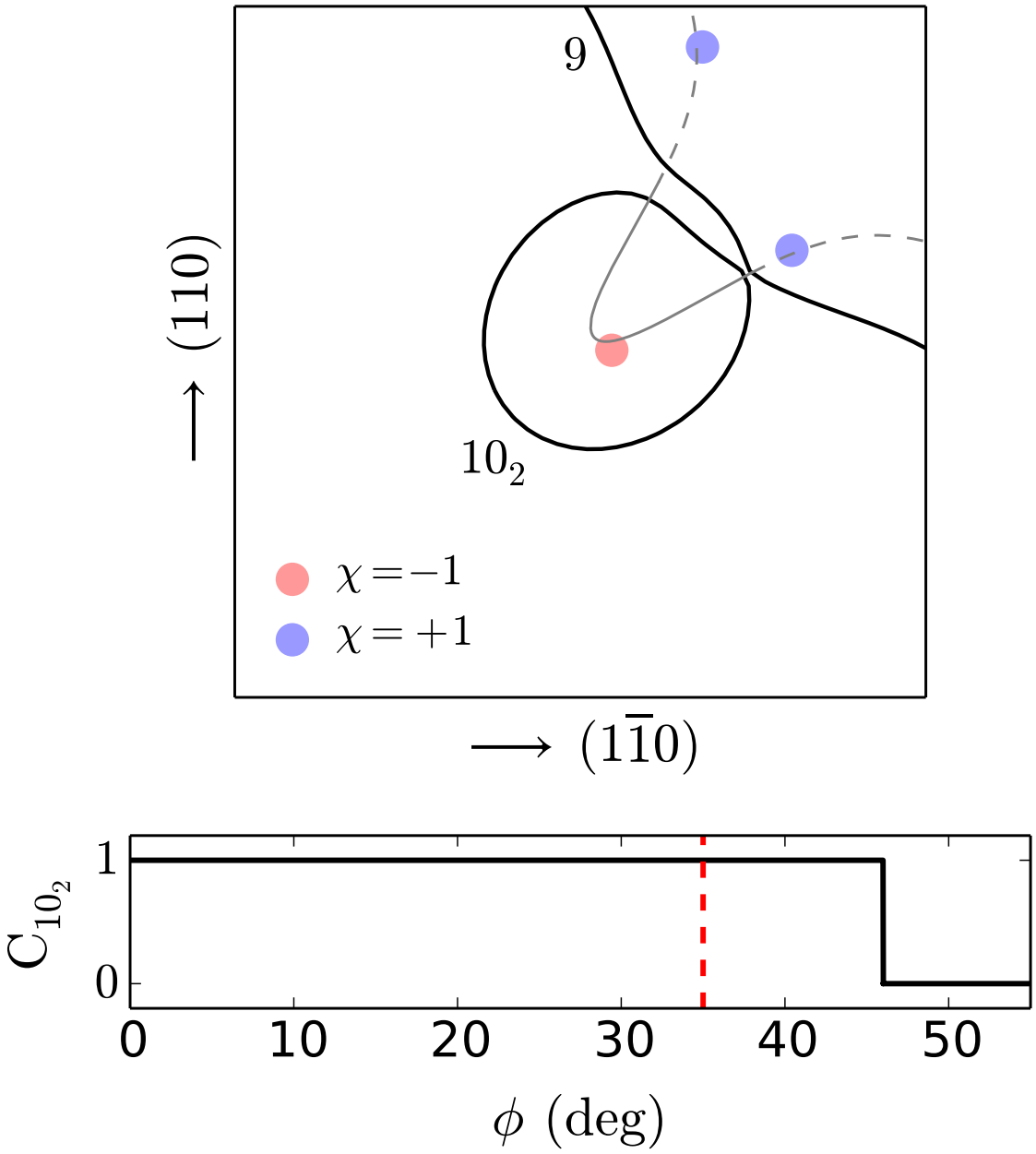

FIG. S8. Upper panel: Fermi contours of bands nine and ten, calculated with the magnetization tilted by 20° (the azimuthal angle ϕ is indicated by the dashed red line in the lower panel). The remnant Weyl points are displayed as colored disks, and the evaporated nodal ring is shown as a guide to the eye. Lower panel: Chern number of pocket 10_2 versus ϕ.

The series of snapshots in Figs. S3-S19 shows the evolution of sheets 9 and 10_2, and the motion of nearby Weyl points (WPs), as the magnetization precesses around [001] (ϕ is the azimuthal precession angle). In order to see clearly the touching between the two sheets at $\phi \simeq 46°$, the Fermi contours are not drawn at exactly $k_z = 0$: in each snapshot their k_z coordinate is pinned to the WP that joins the two sheets at the critical angle (in practice k_z varies only slightly from one snapshot to the next, never deviating by more than $0.004 \times 2\pi/a$ from $k_z = 0$). The touching event leads to a transfer of Chern number between the two sheets, after which the Chern number of pocket 10_2 vanishes as it now encloses two WPs of opposite chirality. The two WPs merge together and annihilate at $\phi \simeq 50°$.

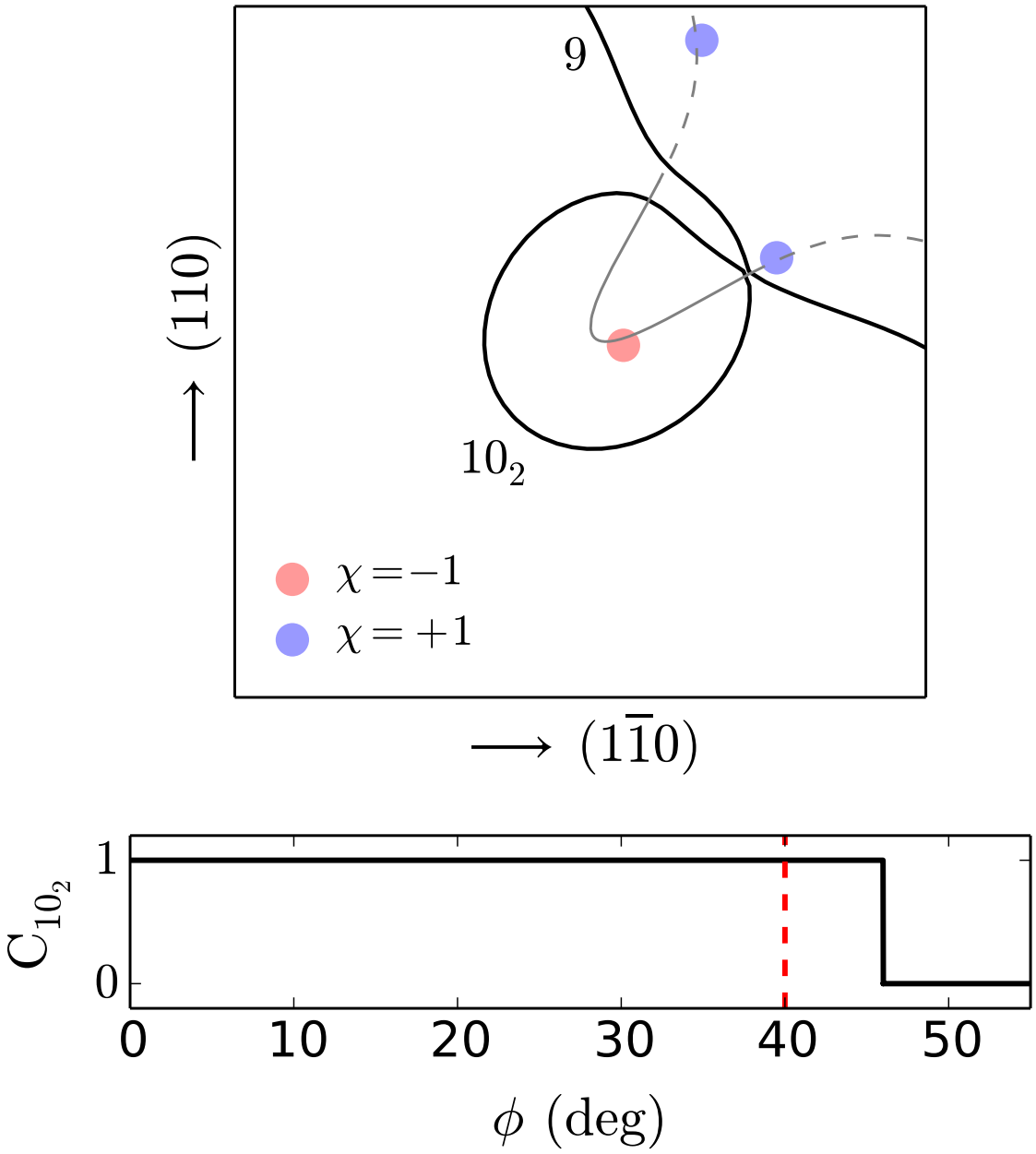

FIG. S9. Upper panel: Fermi contours of bands nine and ten, calculated with the magnetization tilted by 20° (the azimuthal angle ϕ is indicated by the dashed red line in the lower panel). The remnant Weyl points are displayed as colored disks, and the evaporated nodal ring is shown as a guide to the eye. Lower panel: Chern number of pocket 10_2 versus ϕ.

The series of snapshots in Figs. S3-S19 shows the evolution of sheets 9 and 10_2, and the motion of nearby Weyl points (WPs), as the magnetization precesses around [001] (ϕ is the azimuthal precession angle). In order to see clearly the touching between the two sheets at $\phi \simeq 46°$, the Fermi contours are not drawn at exactly $k_z = 0$: in each snapshot their k_z coordinate is pinned to the WP that joins the two sheets at the critical angle (in practice k_z varies only slightly from one snapshot to the next, never deviating by more than $0.004 \times 2\pi/a$ from $k_z = 0$). The touching event leads to a transfer of Chern number between the two sheets, after which the Chern number of pocket 10_2 vanishes as it now encloses two WPs of opposite chirality. The two WPs merge together and annihilate at $\phi \simeq 50°$.

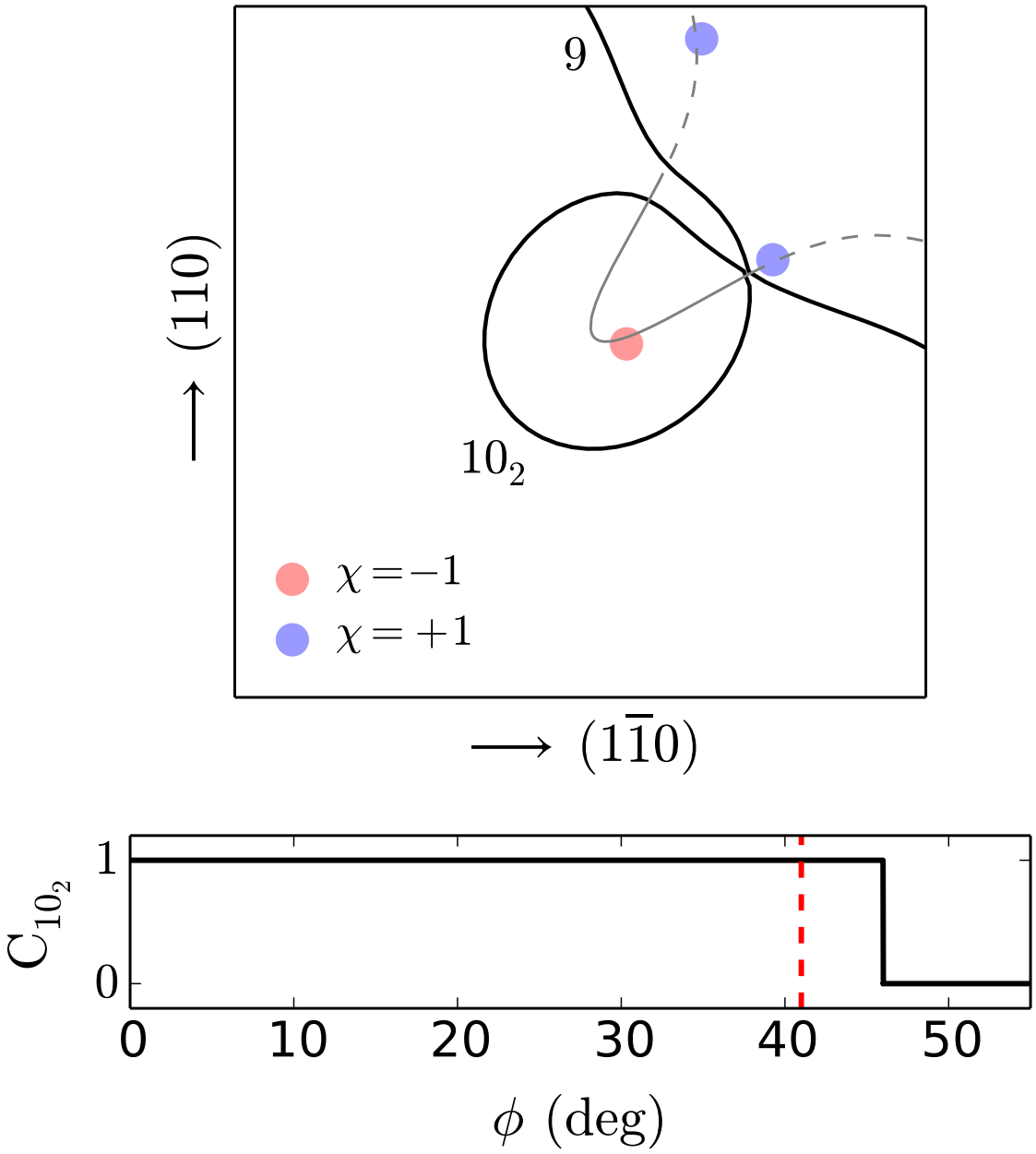

FIG. S10. Upper panel: Fermi contours of bands nine and ten, calculated with the magnetization tilted by 20° (the azimuthal angle ϕ is indicated by the dashed red line in the lower panel). The remnant Weyl points are displayed as colored disks, and the evaporated nodal ring is shown as a guide to the eye. Lower panel: Chern number of pocket 10_2 versus ϕ.

The series of snapshots in Figs. S3-S19 shows the evolution of sheets 9 and 10_2, and the motion of nearby Weyl points (WPs), as the magnetization precesses around [001] (ϕ is the azimuthal precession angle). In order to see clearly the touching between the two sheets at $\phi \simeq 46°$, the Fermi contours are not drawn at exactly $k_z = 0$: in each snapshot their k_z coordinate is pinned to the WP that joins the two sheets at the critical angle (in practice k_z varies only slightly from one snapshot to the next, never deviating by more than $0.004 \times 2\pi/a$ from $k_z = 0$). The touching event leads to a transfer of Chern number between the two sheets, after which the Chern number of pocket 10_2 vanishes as it now encloses two WPs of opposite chirality. The two WPs merge together and annihilate at $\phi \simeq 50°$.

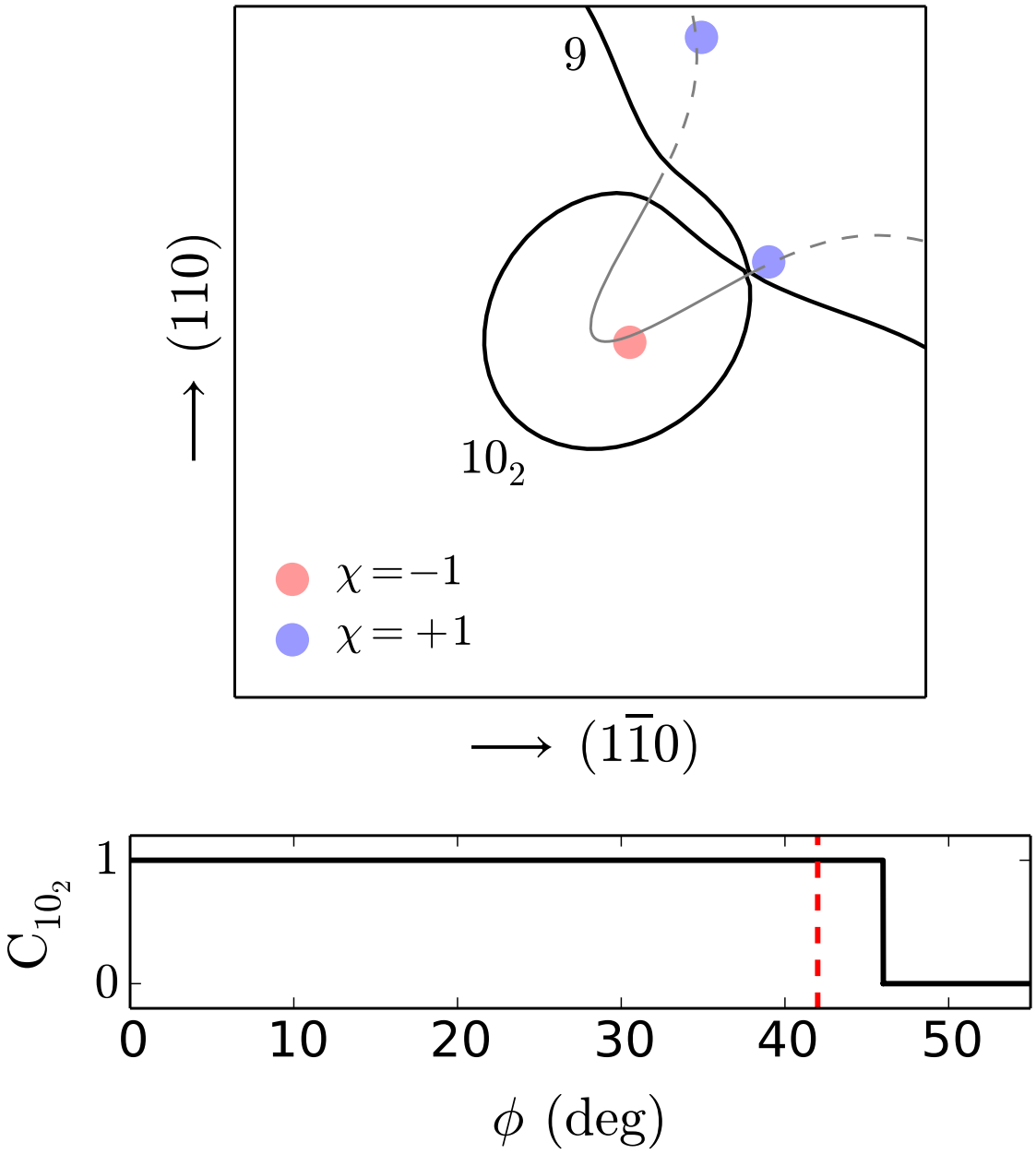

FIG. S11. Upper panel: Fermi contours of bands nine and ten, calculated with the magnetization tilted by 20° (the azimuthal angle ϕ is indicated by the dashed red line in the lower panel). The remnant Weyl points are displayed as colored disks, and the evaporated nodal ring is shown as a guide to the eye. Lower panel: Chern number of pocket 10_2 versus ϕ.

The series of snapshots in Figs. S3-S19 shows the evolution of sheets 9 and 10_2, and the motion of nearby Weyl points (WPs), as the magnetization precesses around [001] (ϕ is the azimuthal precession angle). In order to see clearly the touching between the two sheets at $\phi \simeq 46°$, the Fermi contours are not drawn at exactly $k_z = 0$: in each snapshot their k_z coordinate is pinned to the WP that joins the two sheets at the critical angle (in practice k_z varies only slightly from one snapshot to the next, never deviating by more than $0.004 \times 2\pi/a$ from $k_z = 0$). The touching event leads to a transfer of Chern number between the two sheets, after which the Chern number of pocket 10_2 vanishes as it now encloses two WPs of opposite chirality. The two WPs merge together and annihilate at $\phi \simeq 50°$.

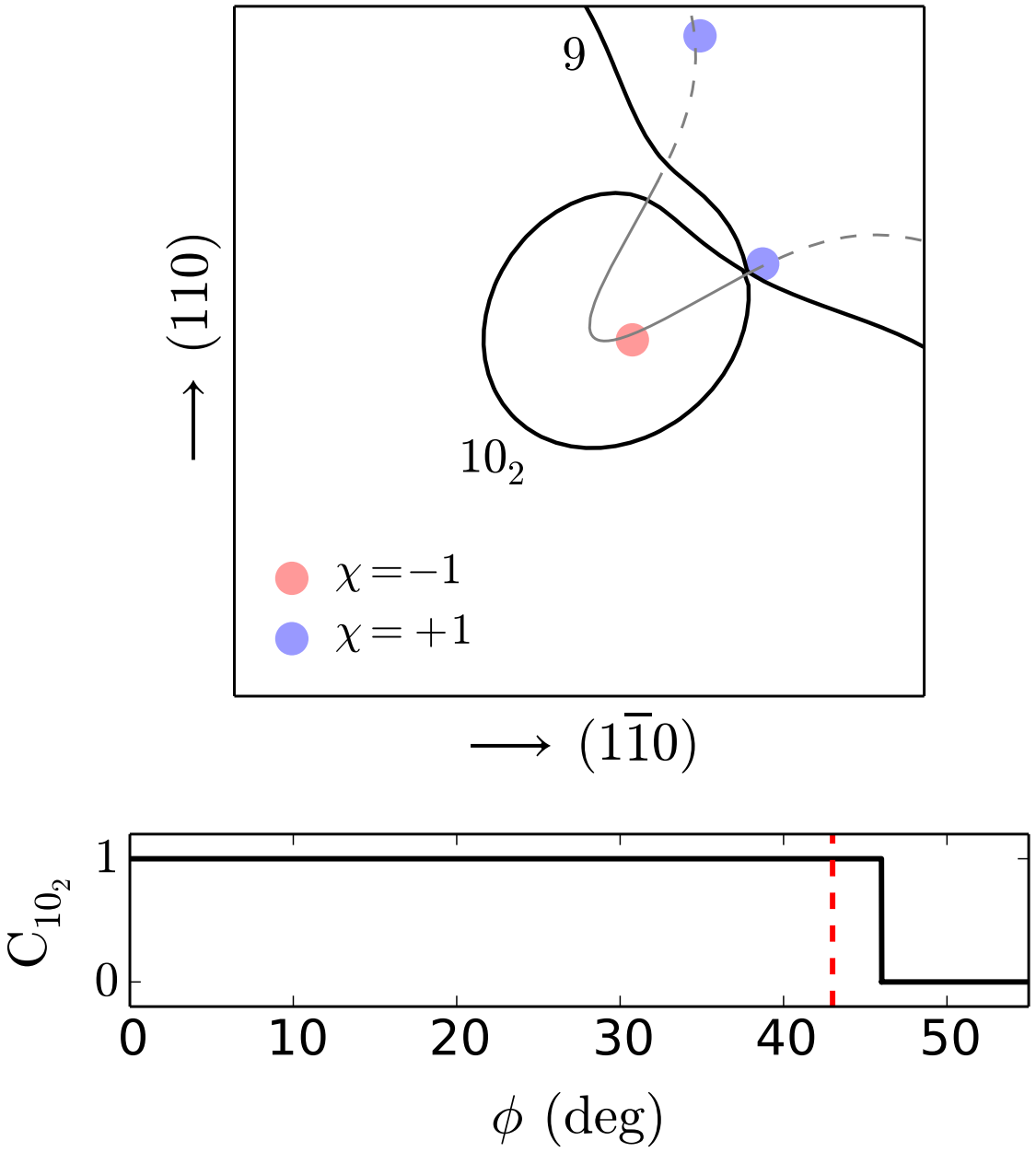

FIG. S12. Upper panel: Fermi contours of bands nine and ten, calculated with the magnetization tilted by 20° (the azimuthal angle ϕ is indicated by the dashed red line in the lower panel). The remnant Weyl points are displayed as colored disks, and the evaporated nodal ring is shown as a guide to the eye. Lower panel: Chern number of pocket 10_2 versus ϕ.

The series of snapshots in Figs. S3-S19 shows the evolution of sheets 9 and 10_2, and the motion of nearby Weyl points (WPs), as the magnetization precesses around [001] (ϕ is the azimuthal precession angle). In order to see clearly the touching between the two sheets at $\phi \simeq 46°$, the Fermi contours are not drawn at exactly $k_z = 0$: in each snapshot their k_z coordinate is pinned to the WP that joins the two sheets at the critical angle (in practice k_z varies only slightly from one snapshot to the next, never deviating by more than $0.004 \times 2\pi/a$ from $k_z = 0$). The touching event leads to a transfer of Chern number between the two sheets, after which the Chern number of pocket 10_2 vanishes as it now encloses two WPs of opposite chirality. The two WPs merge together and annihilate at $\phi \simeq 50°$.

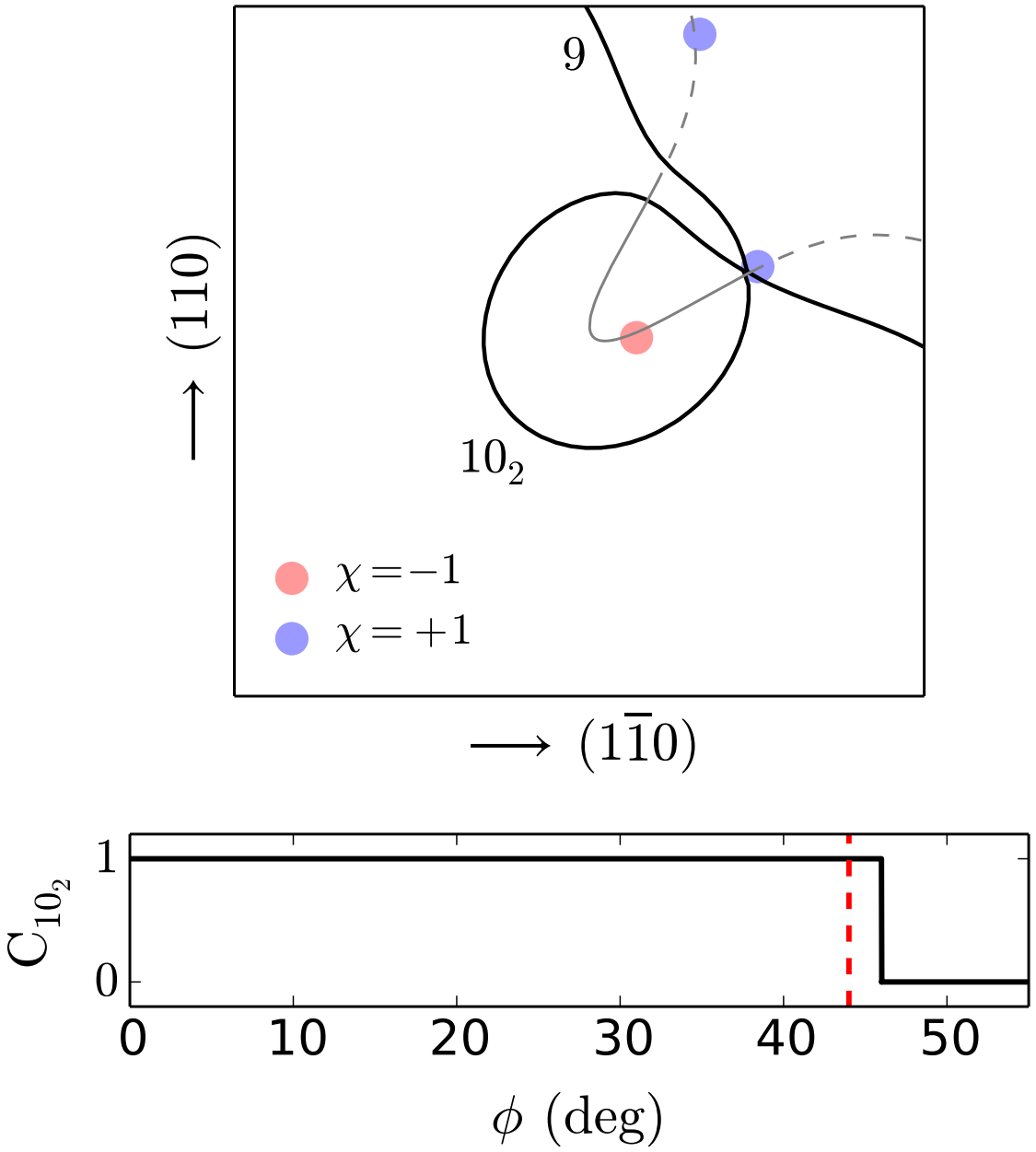

FIG. S13. Upper panel: Fermi contours of bands nine and ten, calculated with the magnetization tilted by 20° (the azimuthal angle ϕ is indicated by the dashed red line in the lower panel). The remnant Weyl points are displayed as colored disks, and the evaporated nodal ring is shown as a guide to the eye. Lower panel: Chern number of pocket 10_2 versus ϕ.

The series of snapshots in Figs. S3-S19 shows the evolution of sheets 9 and 10_2, and the motion of nearby Weyl points (WPs), as the magnetization precesses around [001] (ϕ is the azimuthal precession angle). In order to see clearly the touching between the two sheets at $\phi \simeq 46°$, the Fermi contours are not drawn at exactly $k_z = 0$: in each snapshot their k_z coordinate is pinned to the WP that joins the two sheets at the critical angle (in practice k_z varies only slightly from one snapshot to the next, never deviating by more than $0.004 \times 2\pi/a$ from $k_z = 0$). The touching event leads to a transfer of Chern number between the two sheets, after which the Chern number of pocket 10_2 vanishes as it now encloses two WPs of opposite chirality. The two WPs merge together and annihilate at $\phi \simeq 50°$.

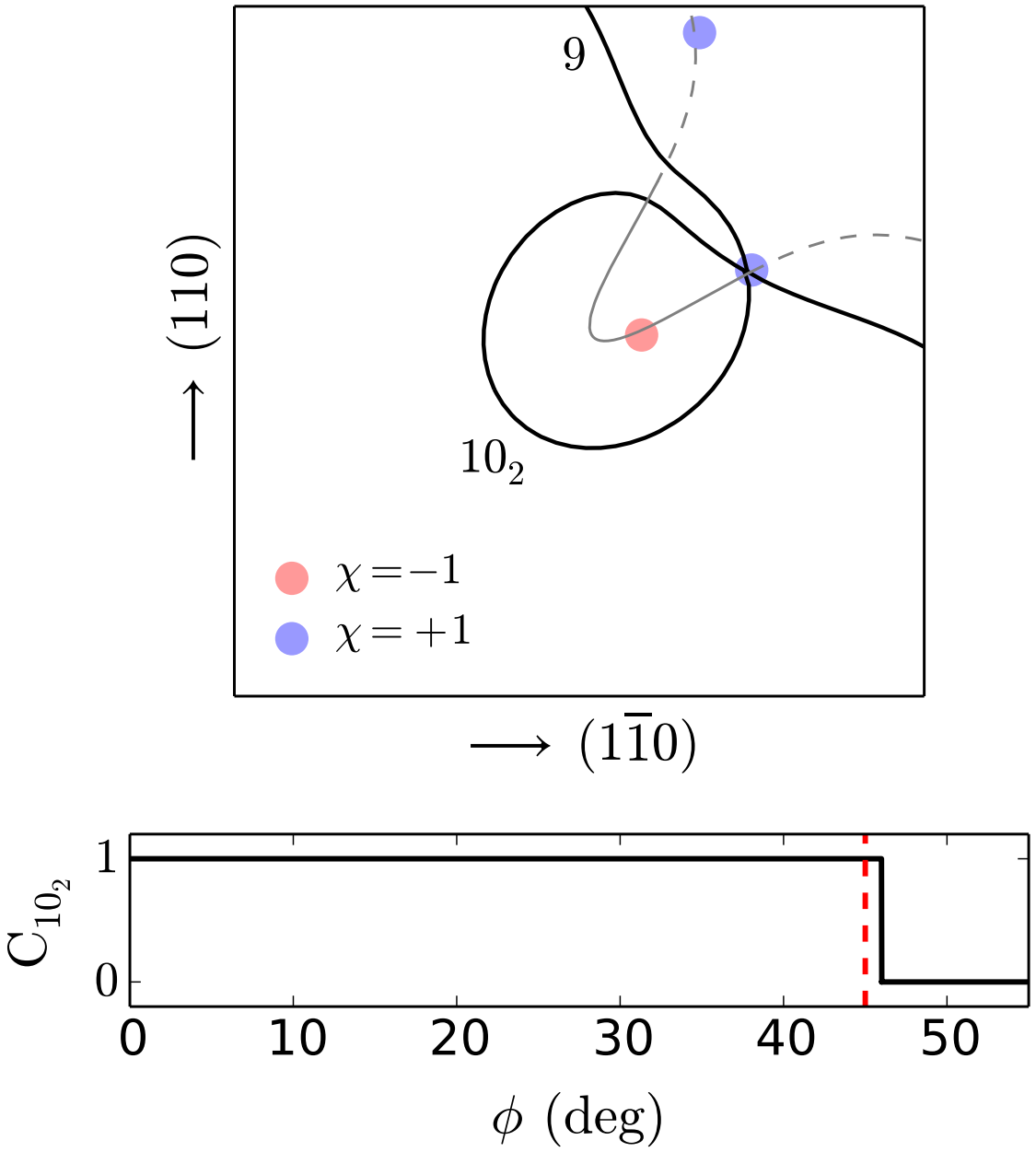

FIG. S14. Upper panel: Fermi contours of bands nine and ten, calculated with the magnetization tilted by 20° (the azimuthal angle ϕ is indicated by the dashed red line in the lower panel). The remnant Weyl points are displayed as colored disks, and the evaporated nodal ring is shown as a guide to the eye. Lower panel: Chern number of pocket 10_2 versus ϕ.

The series of snapshots in Figs. S3-S19 shows the evolution of sheets 9 and 10_2, and the motion of nearby Weyl points (WPs), as the magnetization precesses around [001] (ϕ is the azimuthal precession angle). In order to see clearly the touching between the two sheets at $\phi \simeq 46°$, the Fermi contours are not drawn at exactly $k_z = 0$: in each snapshot their k_z coordinate is pinned to the WP that joins the two sheets at the critical angle (in practice k_z varies only slightly from one snapshot to the next, never deviating by more than $0.004 \times 2\pi/a$ from $k_z = 0$). The touching event leads to a transfer of Chern number between the two sheets, after which the Chern number of pocket 10_2 vanishes as it now encloses two WPs of opposite chirality. The two WPs merge together and annihilate at $\phi \simeq 50°$.

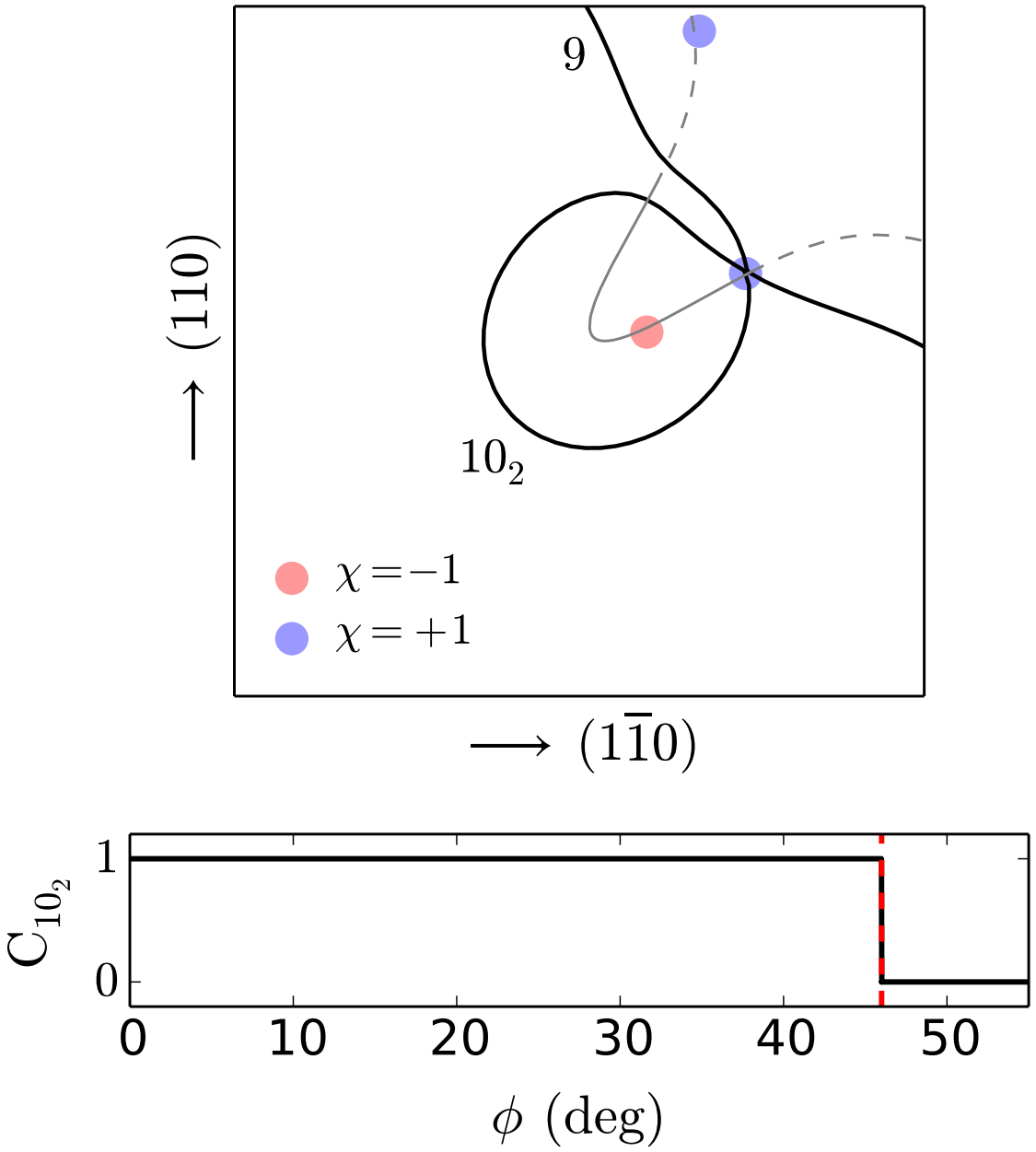

FIG. S15. Upper panel: Fermi contours of bands nine and ten, calculated with the magnetization tilted by 20° (the azimuthal angle ϕ is indicated by the dashed red line in the lower panel). The remnant Weyl points are displayed as colored disks, and the evaporated nodal ring is shown as a guide to the eye. Lower panel: Chern number of pocket 10_2 versus ϕ.

The series of snapshots in Figs. S3-S19 shows the evolution of sheets 9 and 10_2, and the motion of nearby Weyl points (WPs), as the magnetization precesses around [001] (ϕ is the azimuthal precession angle). In order to see clearly the touching between the two sheets at $\phi \simeq 46°$, the Fermi contours are not drawn at exactly $k_z = 0$: in each snapshot their k_z coordinate is pinned to the WP that joins the two sheets at the critical angle (in practice k_z varies only slightly from one snapshot to the next, never deviating by more than $0.004 \times 2\pi/a$ from $k_z = 0$). The touching event leads to a transfer of Chern number between the two sheets, after which the Chern number of pocket 10_2 vanishes as it now encloses two WPs of opposite chirality. The two WPs merge together and annihilate at $\phi \simeq 50°$.

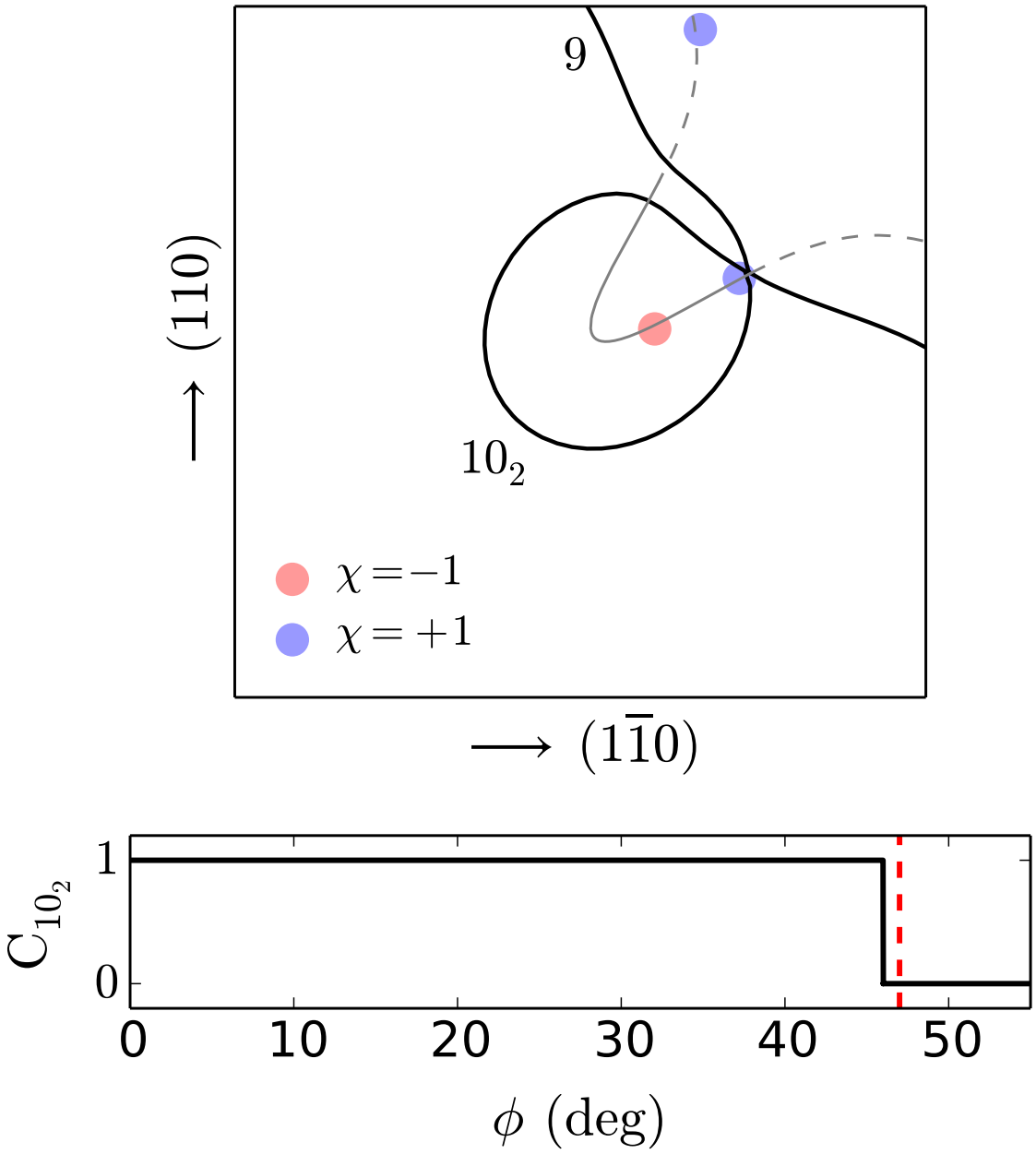

FIG. S16. Upper panel: Fermi contours of bands nine and ten, calculated with the magnetization tilted by 20° (the azimuthal angle ϕ is indicated by the dashed red line in the lower panel). The remnant Weyl points are displayed as colored disks, and the evaporated nodal ring is shown as a guide to the eye. Lower panel: Chern number of pocket 10_2 versus ϕ.

The series of snapshots in Figs. S3-S19 shows the evolution of sheets 9 and 10_2, and the motion of nearby Weyl points (WPs), as the magnetization precesses around [001] (ϕ is the azimuthal precession angle). In order to see clearly the touching between the two sheets at $\phi \simeq 46°$, the Fermi contours are not drawn at exactly $k_z = 0$: in each snapshot their k_z coordinate is pinned to the WP that joins the two sheets at the critical angle (in practice k_z varies only slightly from one snapshot to the next, never deviating by more than $0.004 \times 2\pi/a$ from $k_z = 0$). The touching event leads to a transfer of Chern number between the two sheets, after which the Chern number of pocket 10_2 vanishes as it now encloses two WPs of opposite chirality. The two WPs merge together and annihilate at $\phi \simeq 50°$.

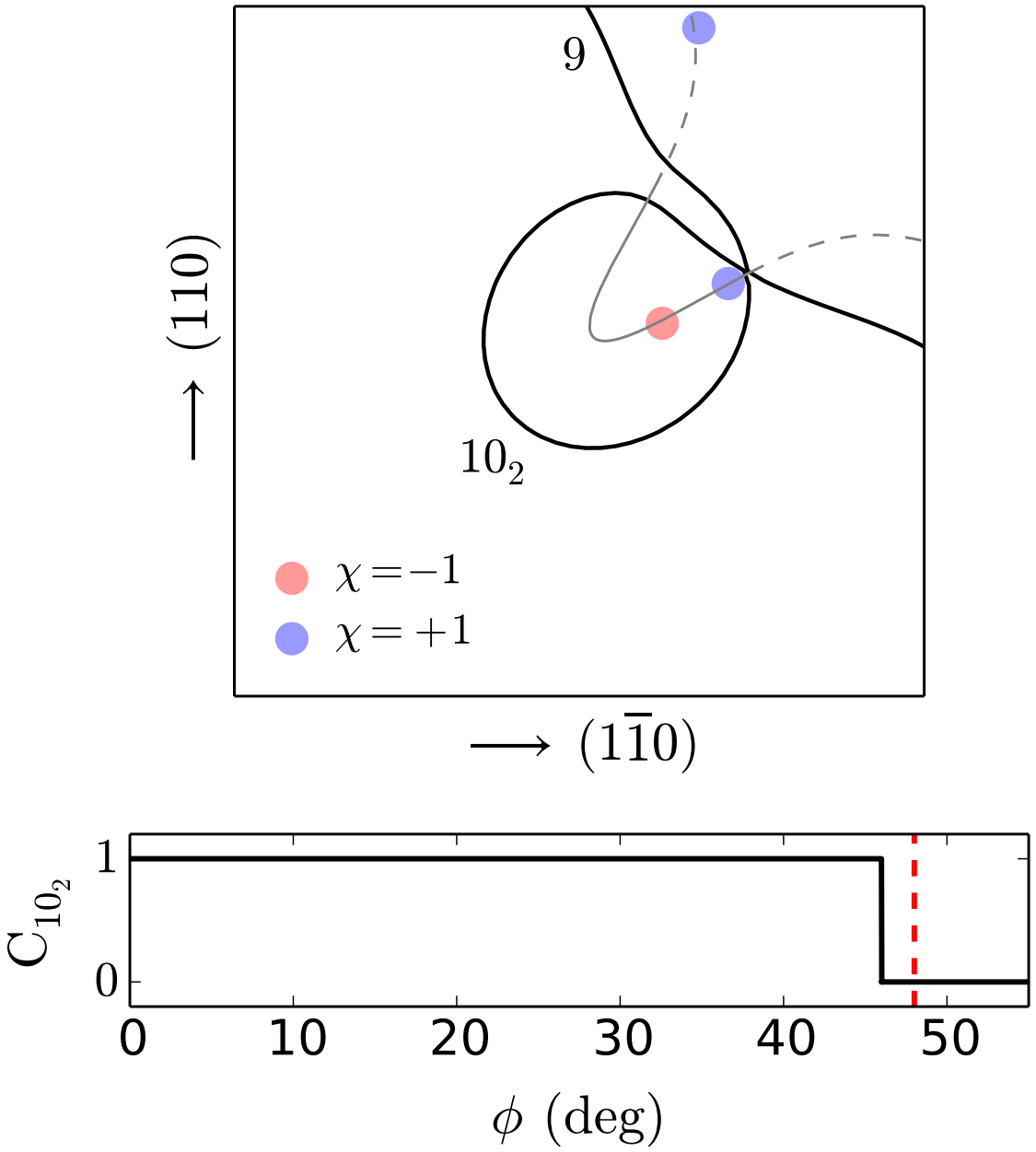

FIG. S17. Upper panel: Fermi contours of bands nine and ten, calculated with the magnetization tilted by 20° (the azimuthal angle ϕ is indicated by the dashed red line in the lower panel). The remnant Weyl points are displayed as colored disks, and the evaporated nodal ring is shown as a guide to the eye. Lower panel: Chern number of pocket 10_2 versus ϕ.

The series of snapshots in Figs. S3-S19 shows the evolution of sheets 9 and 10_2, and the motion of nearby Weyl points (WPs), as the magnetization precesses around [001] (ϕ is the azimuthal precession angle). In order to see clearly the touching between the two sheets at $\phi \simeq 46°$, the Fermi contours are not drawn at exactly $k_z = 0$: in each snapshot their k_z coordinate is pinned to the WP that joins the two sheets at the critical angle (in practice k_z varies only slightly from one snapshot to the next, never deviating by more than $0.004 \times 2\pi/a$ from $k_z = 0$). The touching event leads to a transfer of Chern number between the two sheets, after which the Chern number of pocket 10_2 vanishes as it now encloses two WPs of opposite chirality. The two WPs merge together and annihilate at $\phi \simeq 50°$.

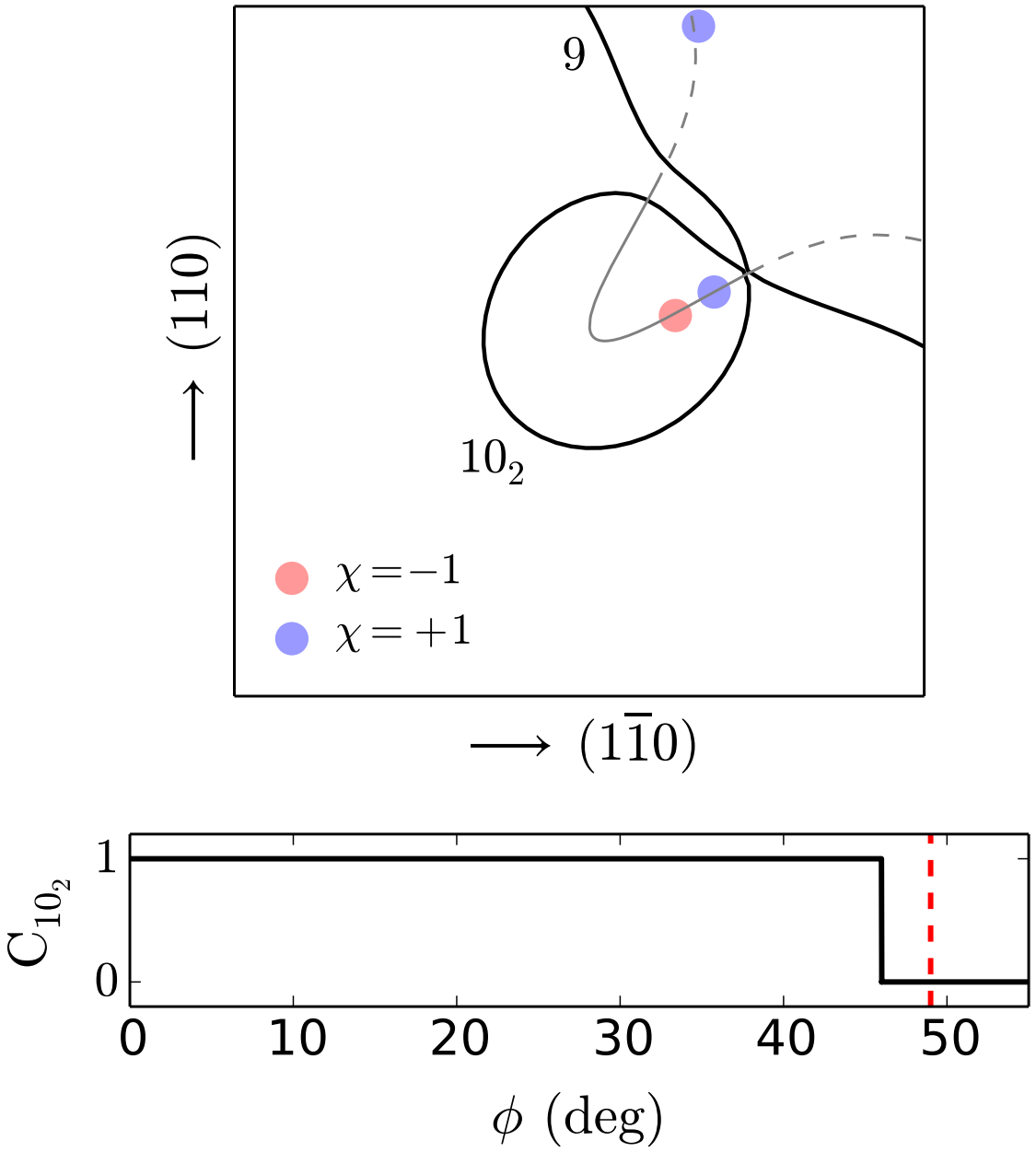

FIG. S18. Upper panel: Fermi contours of bands nine and ten, calculated with the magnetization tilted by 20° (the azimuthal angle ϕ is indicated by the dashed red line in the lower panel). The remnant Weyl points are displayed as colored disks, and the evaporated nodal ring is shown as a guide to the eye. Lower panel: Chern number of pocket 10_2 versus ϕ.

The series of snapshots in Figs. S3-S19 shows the evolution of sheets 9 and 10_2, and the motion of nearby Weyl points (WPs), as the magnetization precesses around [001] (ϕ is the azimuthal precession angle). In order to see clearly the touching between the two sheets at $\phi \simeq 46°$, the Fermi contours are not drawn at exactly $k_z = 0$: in each snapshot their k_z coordinate is pinned to the WP that joins the two sheets at the critical angle (in practice k_z varies only slightly from one snapshot to the next, never deviating by more than $0.004 \times 2\pi/a$ from $k_z = 0$). The touching event leads to a transfer of Chern number between the two sheets, after which the Chern number of pocket 10_2 vanishes as it now encloses two WPs of opposite chirality. The two WPs merge together and annihilate at $\phi \simeq 50°$.

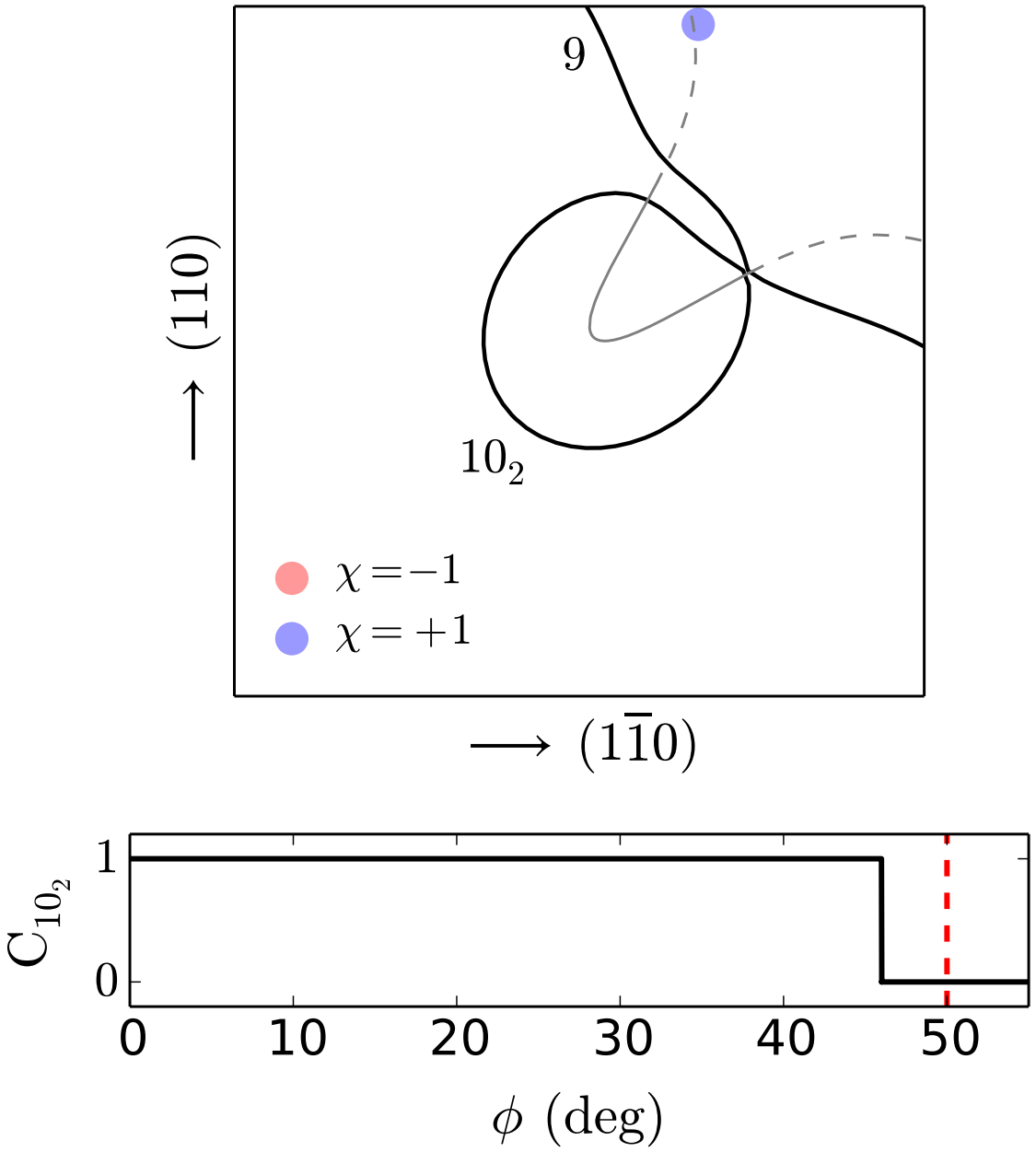

FIG. S19. Upper panel: Fermi contours of bands nine and ten, calculated with the magnetization tilted by 20° (the azimuthal angle ϕ is indicated by the dashed red line in the lower panel). The remnant Weyl points are displayed as colored disks, and the evaporated nodal ring is shown as a guide to the eye. Lower panel: Chern number of pocket 10_2 versus ϕ.

II. CHIRAL TOUCHING BETWEEN FERMI SHEETS UPON VARYING THE FERMI LEVEL

The results in this section were obtained with the magnetization along the easy axis [001]. Figure S20 shows the Fermi contours of bands nine and ten on the ΓNP ($k_x = k_y$) plane in Fig. 3. Pockets 9 and 10_1 have zero Chern number, and pockets 10_6 and 10_7 have Chern numbers -1 and $+1$ (see Table III). The series of snapshots in Figs. S21-S25 depicts the touching event between sheets 9 and 10_7 upon increasing the Fermi level, leading to a transfer of Chern number between them (Sec. VI.C.2).

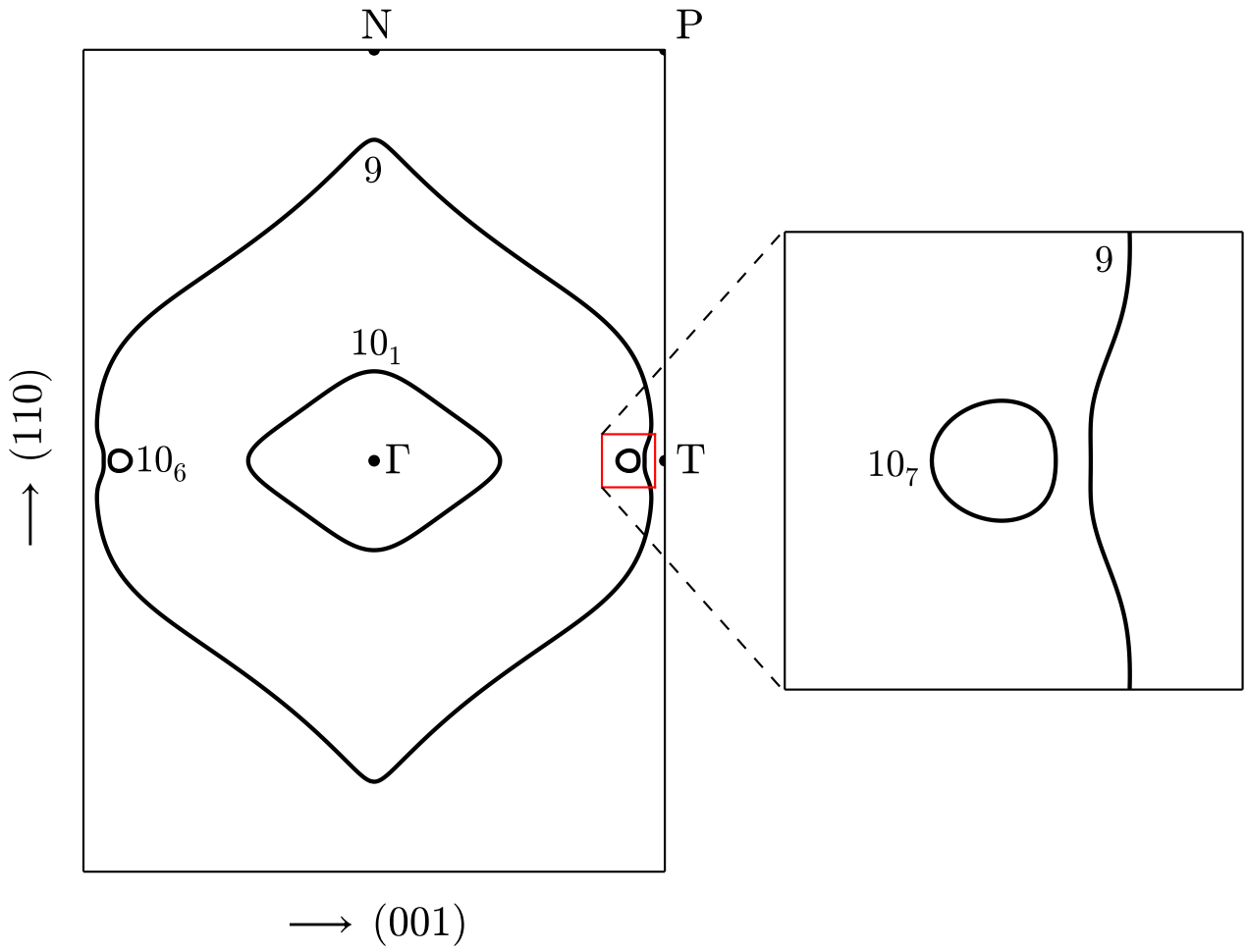

FIG. S20. Left: Fermi contours of bands nine and ten on the ΓNP Brillouin-zone slice at $k_x = k_y$, evaluated for the true (unshifted) Fermi level. Right: Detail showing the region of closest approach between sheets 9 and 10_7.

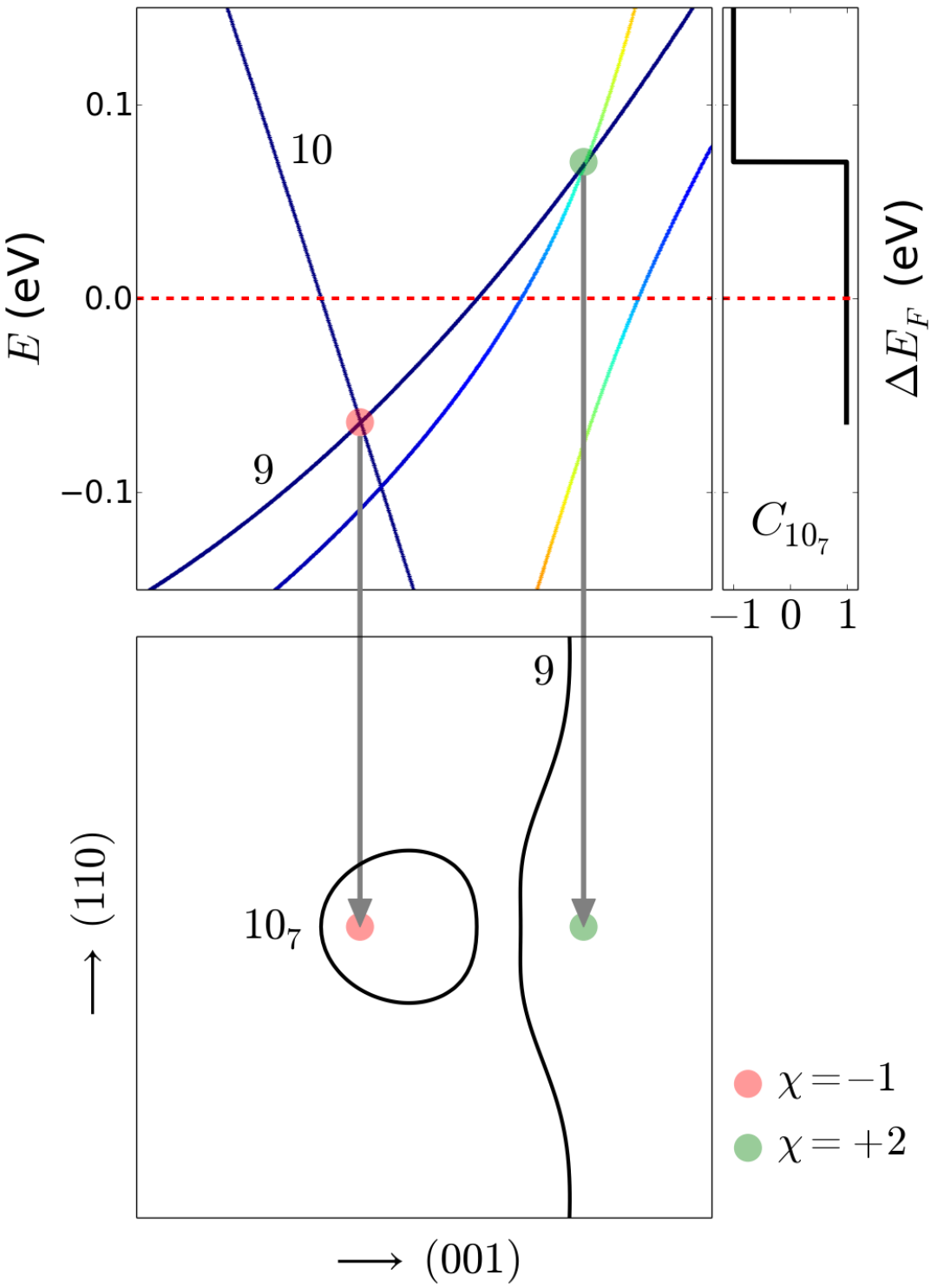

FIG. S21. Upper-left panel: Energy bands along the line Δ in Fig. 3, close to the electron pocket 10_7 [see also Fig. 13(a)]. Energies are measured from the true Fermi level. Upper-right panel: Chern number of pocket 10_7 versus the Fermi-level shift. Lower panel: Fermi contours inside the red square in Fig. S20 for $\Delta E_F = 0.000$ eV (the dashed red line in the upper panels). The colored disks represent Weyl nodes between bands nine and ten, with chiral charges χ .

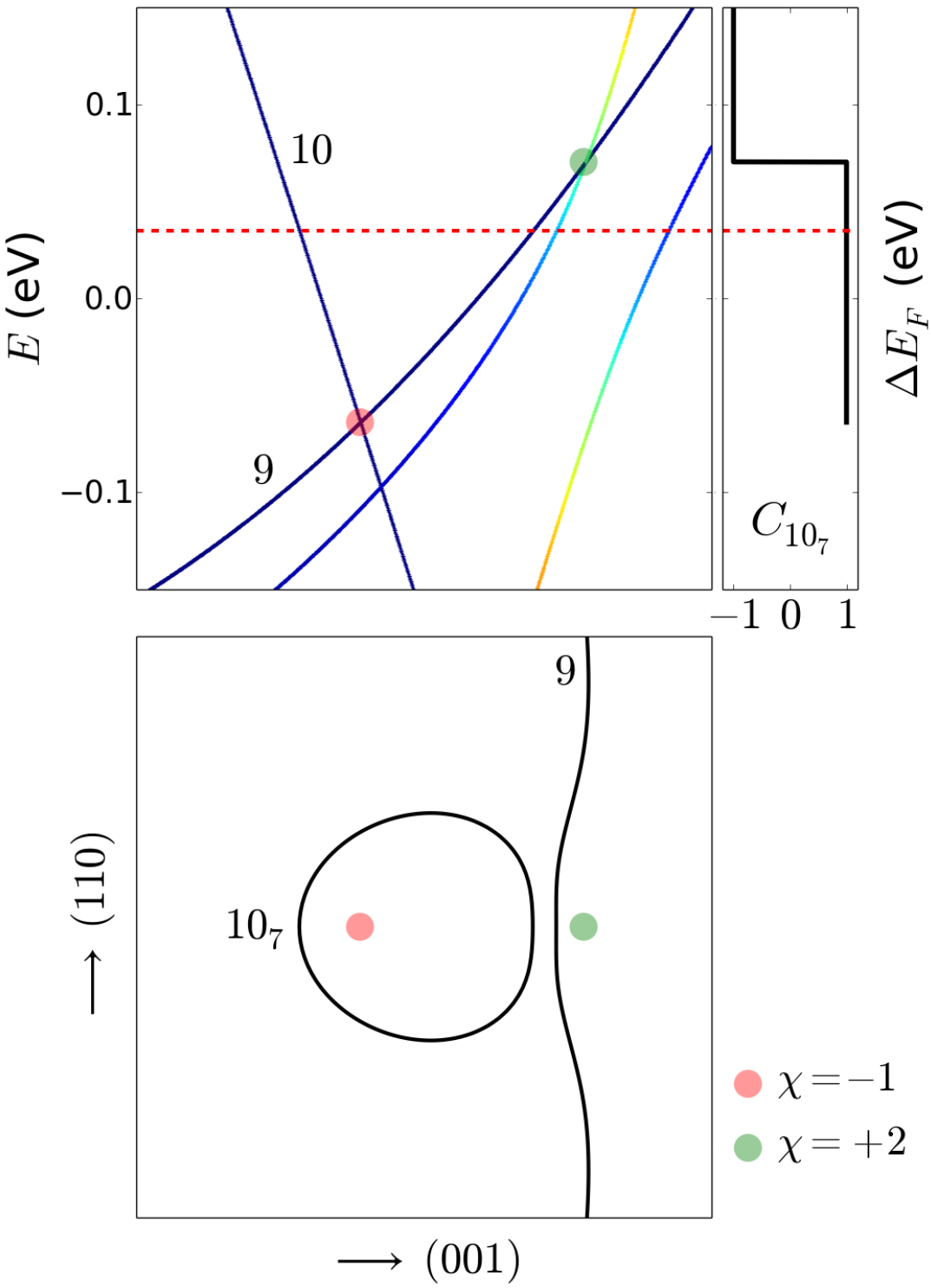

FIG. S22. Upper-left panel: Energy bands along the line Δ in Fig. 3, close to the electron pocket 10_7 [see also Fig. 13(a)]. Energies are measured from the true Fermi level. Upper-right panel: Chern number of pocket 10_7 versus the Fermi-level shift. Lower panel: Fermi contours inside the red square in Fig. S20 for $\Delta E_F = 0.035$ eV (the dashed red line in the upper panels). The colored disks represent Weyl nodes between bands nine and ten, with chiral charges χ .

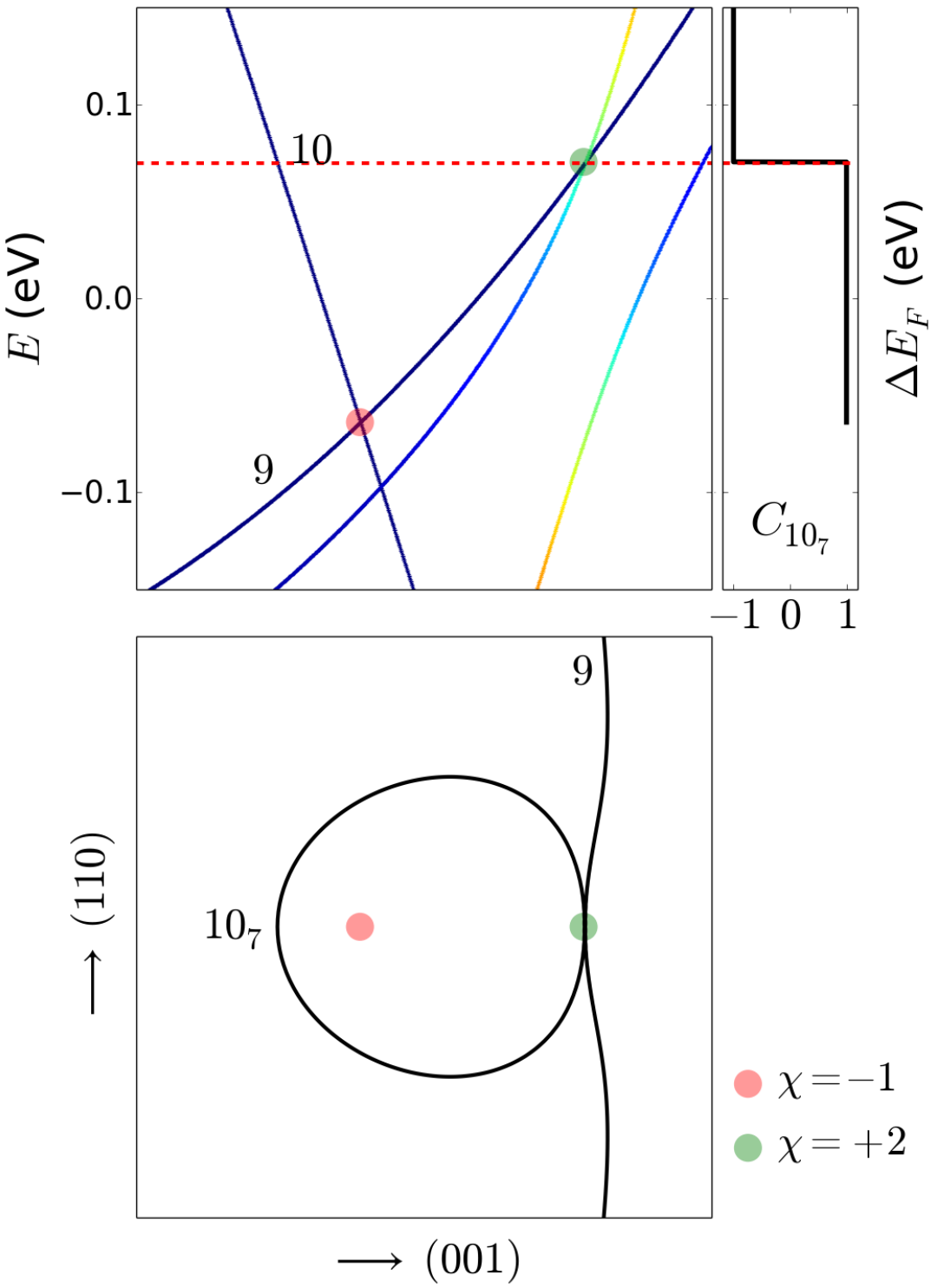

FIG. S23. Upper-left panel: Energy bands along the line Δ in Fig. 3, close to the electron pocket 10_7 [see also Fig. 13(a)]. Energies are measured from the true Fermi level. Upper-right panel: Chern number of pocket 10_7 versus the Fermi-level shift. Lower panel: Fermi contours inside the red square in Fig. S20 for $\Delta E_F = 0.070$ eV (the dashed red line in the upper panels). The colored disks represent Weyl nodes between bands nine and ten, with chiral charges χ .

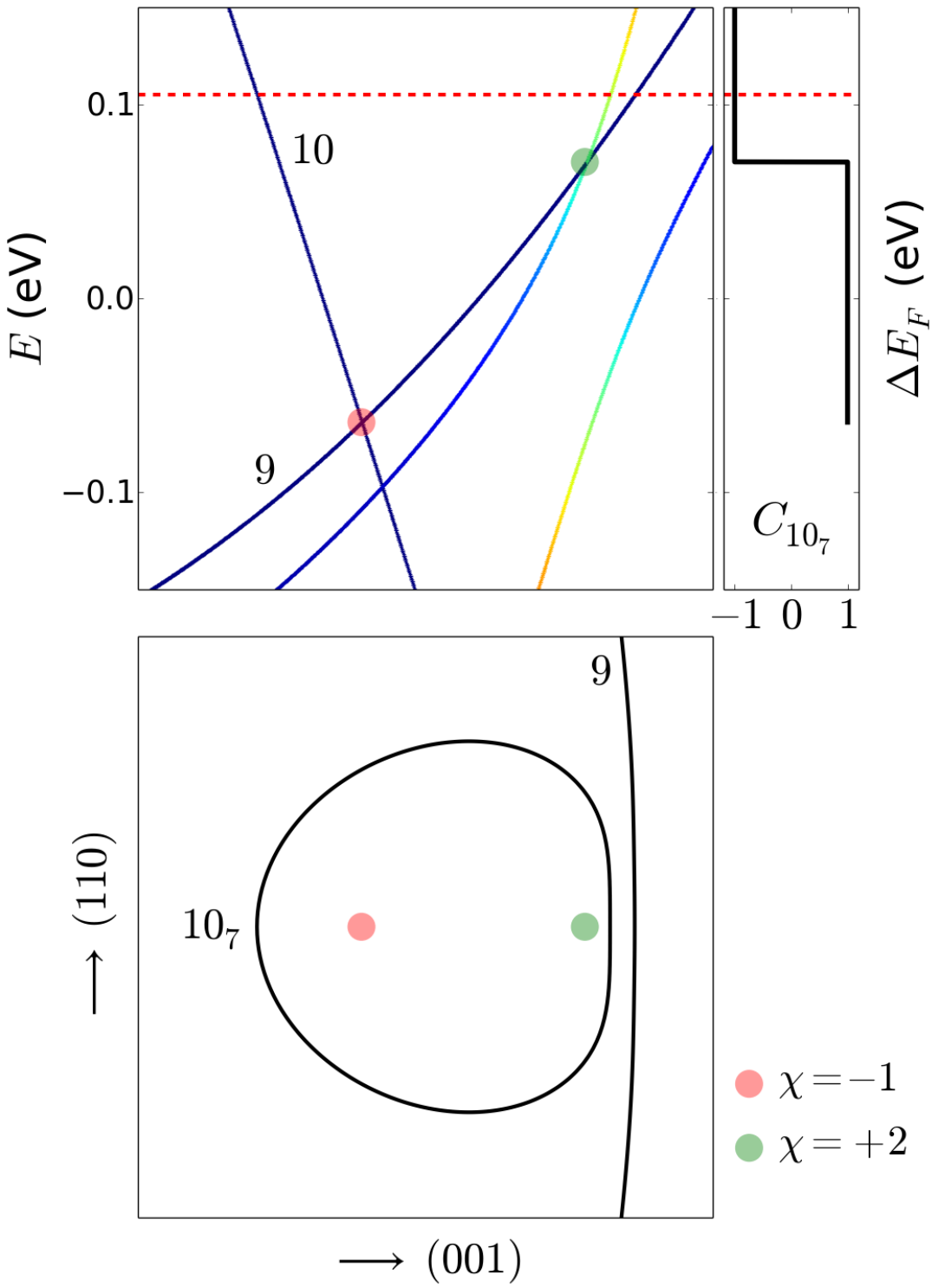

FIG. S24. Upper-left panel: Energy bands along the line Δ in Fig. 3, close to the electron pocket 10_7 [see also Fig. 13(a)]. Energies are measured from the true Fermi level. Upper-right panel: Chern number of pocket 10_7 versus the Fermi-level shift. Lower panel: Fermi contours inside the red square in Fig. S20 for $\Delta E_F = 0.105$ eV (the dashed red line in the upper panels). The colored disks represent Weyl nodes between bands nine and ten, with chiral charges χ .

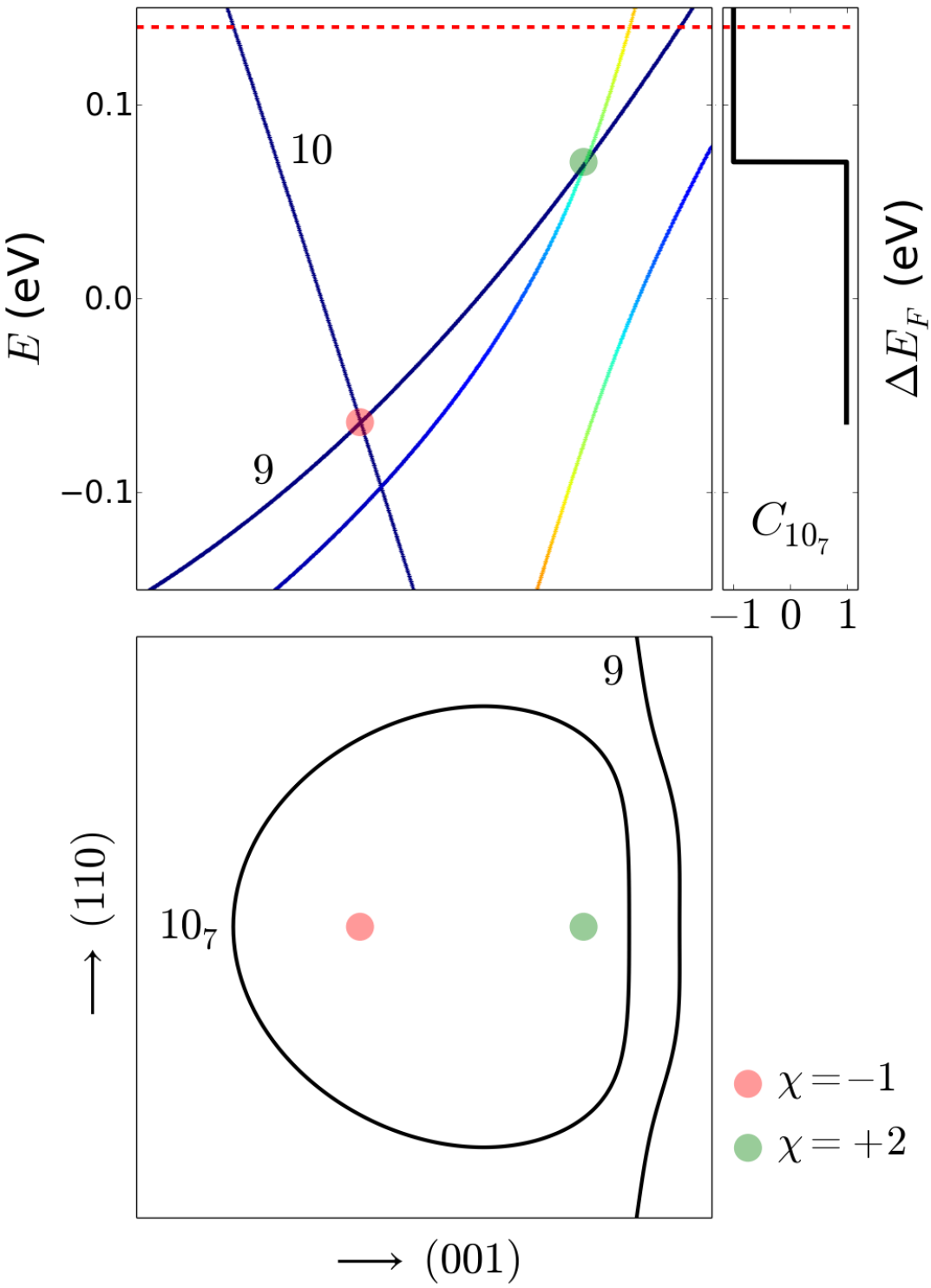

FIG. S25. Upper-left panel: Energy bands along the line Δ in Fig. 3, close to the electron pocket 10_7 [see also Fig. 13(a)]. Energies are measured from the true Fermi level. Upper-right panel: Chern number of pocket 10_7 versus the Fermi-level shift. Lower panel: Fermi contours inside the red square in Fig. S20 for $\Delta E_F = 0.140$ eV (the dashed red line in the upper panels). The colored disks represent Weyl nodes between bands nine and ten, with chiral charges χ .